Neurotherapeutics 21 (2024) e00301

Contents lists available at ScienceDirect

Neurotherapeutics

journal homepage: www.sciencedirect.com/journal/neurotherapeutics

Original Article

Nicotinamide riboside, pterostilbene and ibudilast protect motor neurons and extend survival in ALS mice

Rafael López-Blanch [a,b], Rosario Salvador-Palmer [a], María Oriol-Caballo [a,b], Paz Moreno-Murciano [b], Ryan W. Dellinger [c], José M. Estrela [a,b,d,*], Elena Obrador [a,b,*]

[a] Department of Physiology, Faculty of Medicine & Odontology, University of Valencia, 46010 Valencia, Spain
[b] Scientia BioTech, 46002 Valencia, Spain
[c] Elysium Health Inc., New York, NYC 10004, USA
[d] Department of Physiology, Faculty of Pharmacy, University of Valencia, 46100 Burjassot, Spain

ARTICLE INFO

Keywords:
Amyotrophic lateral sclerosis
Motor neurons
Oxidative stress
Nitric oxide
Neuroinflammation
NAD^+

ABSTRACT

Oxidative stress and neuroinflammation are major contributors to the pathophysiology of ALS. Nicotinamide riboside (a NAD^+ precursor) and pterostilbene (a natural antioxidant) were efficacious in a human pilot study of ALS patients and in ALS $SOD1^{G93A}$ transgenic mice. Ibudilast targets different phosphodiesterases and the macrophage migration inhibitory factor, reduces neuroinflammation, and in early-phase studies improved survival and slowed progression in ALS patients. Using two ALS murine models ($SOD1^{G93A}$, FUS^{R521C}) the effects of nicotinamide riboside, pterostilbene, and ibudilast on disease onset, progression and survival were studied. In both models ibudilast enhanced the effects of nicotinamide riboside and pterostilbene on survival and neuromotor functions. The triple combination reduced microgliosis and astrogliosis, and the levels of different proinflammatory cytokines in the CSF. TNFα, IFNγ and IL1β increased H_2O_2 and NO generation by motor neurons, astrocytes, microglia and endothelial cells isolated from ALS mice. Nicotinamide riboside and pterostilbene decreased H_2O_2 and NO generation in all these cells. Ibudilast specifically decreased TNFα levels and H_2O_2 generation by microglia and endothelial cells. Unexpectedly, pathophysiological concentrations of H_2O_2 or NO caused minimal motor neuron cytotoxicity. H_2O_2-induced cytotoxicity was increased by NO via a trace metal-dependent formation of potent oxidants (i.e. OH and ^-OONO radicals). In conclusion, our results show that the combination of nicotinamide riboside, pterostilbene and ibudilast improve neuromotor functions and survival in ALS murine models. Studies on the underlying mechanisms show that motor neuron protection involves the decrease of oxidative and nitrosative stress, the combination of which is highly damaging to motor neurons.

Introduction

Oral administration of nicotinamide riboside (NR) and pterostilbene (PT) has been shown to synergistically increase the survival of amyotrophic lateral sclerosis (ALS $SOD1^{G93A}$ mice (expressing a mutant form of human SOD1) as well as ameliorate ALS-associated loss of neuromotor functions [1]. The increased survival in these mice was accompanied with a delayed onset of symptoms, i.e. functional performance and neuromotor coordination. Histopathology revealed significantly reduced motor neuron (MN) degeneration in mice treated with NR + PT versus controls. Analysis of MNs isolated from these mice showed that NR + PT protected against TNFα-induced oxidative stress and demonstrated induction of Nrf2-dependent antioxidant defenses as well as increase in sirtuins [1]. These results suggested the involvement of oxidative stress, neuroinflammation, specific Nrf2-dependent antioxidant defenses, NAD^+ and sirtuins in the pathophysiology of ALS.

The efficacy of NR + PT as a potential treatment for ALS was also shown in a placebo-controlled double-blind human pilot study in ALS patients [2] (NCT03489200). In this study, NR + PT treatment significantly slowed the progression of ALS as measured by ALSFRS-R score, forced vital capacity and Medical Research Council grading scale when compared to the placebo group [2]. These results showed that NR + PT may be a viable treatment for ALS by protecting MN from degeneration and reducing oxidative stress.

* Corresponding authors.
E-mail addresses: jose.m.estrela@uv.es (J.M. Estrela), elena.obrador@uv.es (E. Obrador).

https://doi.org/10.1016/j.neurot.2023.10.011
Received 9 October 2023; Received in revised form 27 October 2023; Accepted 30 October 2023

Neuroinflammation, involving reactive astrocytes and microglia, infiltration of peripheral immune cells, and increased levels of inflammatory mediators, affects motor regions of the central nervous system (CNS) in ALS [3]. Reactive glial and infiltrating immune cells potentially generate high levels of reactive oxygen species (ROS) [4]. Although ROS are not considered a cause of ALS, they may exacerbate the damage to MNs [1] and to neuromuscular junctions [5]. Moreover, high levels of ROS have been suggested to cause dysfunction of the vascular endothelium, tissue injury and more inflammation [6], a cascade of pathological events which could generate a vicious circle favoring the damage to MNs. Furthermore, mitochondrial dysfunction has also been implicated as a key neuropathological hallmark of ALS [7], including e.g. reduction of the activity of the electron transport chain complexes (complex I–IV) in post-mortem spinal cord specimens from SALS patients [8], reduced intracellular ATP levels in lymphocytes of ALS patients [9], inhibition of the voltage-dependent anion channel (VDAC) by mutant SOD1 [10], deactivation of mitochondrial sirtuin activities [11], or defects involving the autophagy/mitophagy mechanisms [12].

It is known that cyclic nucleotide phosphodiesterase (PDE) inhibitors can diminish glial cell activation [13]. Consequently, PDE inhibitors have been proposed as a possible anti-inflammatory strategy for ALS [14]. One of these inhibitors, ibudilast (IBU, an inhibitor of macrophage migration inhibitory factor and of PDE 3, 4, 10, and 11, but inhibiting the PDE4 subtype to the greatest extent) [15], is currently being assayed in ALS patients (NCT04057898, COMBAT-ALS).

The aim of this contribution was to investigate whether IBU could enhance the protective effects of the NR and PT combination. For this purpose, we used two accepted murine ALS models which develop severe motor neuron impairment at a young age. SOD1^{G93A} transgenic mice express a G93A mutant form of human SOD1. SOD1^{G93A} mice develop neurodegeneration of spinal motor neurons and progressive motor deficits leading to paralysis [16], being neuromotor alterations significant at postnatal week 12 (symptomatology onset) and well established at weeks 17-18 (advanced state of progression) [1]. FUS^{R521C} mice develops robust neuronal loss in the spinal cord, denervation of neuromuscular junctions, and muscle atrophy. The majority of the transgenic FUS^{R521C} protein in these mice is mislocalized to the cytoplasm [17]. The onset of the symptomatology is around postnatal week 7 in FUS^{R521C} mice and well established at weeks 17–19 (advanced state of progression) [18].

Methods

Mice

Mice (female) were from the Jackson Laboratory (Mount Desert Island, ME). B6.CgTg(SOD1*G93A)1Gur/J mice (https://www.jax.org/strain/004435) are hemizygous for the SOD1G93A transgene with transgenic expression of a G93A mutant form of human SOD1. B6.SJL-Tg(Prnp-FUS*R521C)3313Ejh/J mice (https://www.jax.org/strain/026406) express the transgenic FUS^{R521C} protein which aggregates in the cytoplasm. Procedures were in compliance with international laws and policies (EEC Directive 86/609, OJ L 358.1, December 12, 1987; and NIH Guide for the Care and Use of Laboratory Animals, NIH Publ. No. 85-23, 1985). Mice were kept on a 12-h-light/12-h-dark cycle with the room temperature at 22 °C. All mice used in our studies were 4 weeks old (14–16 g) at the beginning of the experimental procedures, and were randomly distributed among the different experimental groups. Evaluation of their health status was based on NIH standards (www.nih.gov). The cages of the animals were housed in a SPF area. Dried pelleted standard rodent chow (Altromin®, Germany) and normal tap water were available to the animals *ad libitum*. Experiments were performed respecting the principles of the 3Rs (Committee of Ethics in Animal Experimentation of our institution).

Nicotinamide riboside, pterostilbene and ibudilast administration

NR was administered orally: 185 mg of NR/kg (dissolved in physiological saline and given as a single dose per day with the help of a micropipette tip; the volume administered was 25 μL per mouse). PT was administered with the feed: 30 mg of PT/kg × day [1]. IBU (12 mg/kg x day, single dose) (Merck, Taufkirchen, Germany) was dissolved in physiological saline and administered orally (directly into the animal's mouth with the help of a tip). The procedure did not require sedation and anesthesia. Administration of all compounds was carried out between 10.00 and 10.30 a.m. in the animal facilities of our institution. NR and PT and/or IBU administration started 4 weeks after birth. Wild-type (WT) B6SJLF1/J [produced by a cross between a C57BL/6J (B6) female × and an SJL/J (SJL) male] (www.jax.org) were used as WT controls. These WT mice were treated with NR + PT, IBU and NR + PT + IBU (same doses and timing used for the ALS models) and we found no changes in neuromotor functionality, cytokine levels in the CSF or the number of MNs in the grey matter of the ventral horns, as compared to untreated WT mice. These tests (see below) were performed at the times where the onset of the symptomatology or an advanced state of progression is observed in the ALS models. Thus indicating that treatment with NR, PT and IBU does not cause toxicity *per se*.

Assessment of neuromotor functionality

Neuromotor functions were evaluated following previously described standard tests [1]. The neurological score was based on the scale of Weydt et al. [19], where "0" indicates a healthy mouse with no classical signs of ALS; "1" indicates the presence of tremors in the hind legs that occur in early disease stage; "2" indicates that mice have difficulty in separating their hind legs when suspended by their tails, which is indicative of muscle weakness; "3" is given when mice exhibit difficulty walking, either stumbling or wobbling; "4" is given when mice were unable to walk on all four legs and drag their hind legs; "5" is given when mice were unable to right themselves after 30 s. Reaching a score of "5," the animals are euthanized for ethical reasons. The rotarod test (Rota Rod, Harvard Apparatus, Holliston, MA) evaluated balance, grip strength, and neuromotor coordination of the mice. For this test each animal was given three trials and the maximum period (seconds) that it could remain on a rotating axle (3.5 cm diameter; speed of rotation, 15 rpm) without falling was measured. Each mouse was given up to three attempts for an arbitrary limit of 1200 s and the longest period was recorded. Changes over time in the different groups were monitored weekly.

Pathology

At 17–18 weeks (SOD1 ^{G93A}) or 17–19 weeks (FUS^{R521C}) of age, 4–5 mice per group were perfused through the left ventricle with ice-cold paraformaldehyde (4 %) in PBS (pH 7.4). The lumbar and thoracic segments of the medulla were surgically isolated, post-fixed for 24 h, and paraffin embedded. Segments were serially cut [2-μm-thick slices, 20 cuts at different levels (L2–L5, T5–T10] using a Leica RM2255 microtome (Leica Biosystems, Wetzlar, Germany). Sections were stained with hematoxylin and eosin. MNs were immunohistochemically stained with anti-choline acetyltransferase antibody (rabbit anti-ChAT polyclonal antibody AB143, Millipore, Burlington, MA). Microglia was immunohistochemically stained using anti-ionized calcium-binding adapter molecule 1 (Iba1) monoclonal antibodies (mAbs) (ab5076, Abcam, Cambridge, UK). Astroglia was immunohistochemical stained using anti-glial fibrillary acidic protein (GFAP) mAbs (ab8975, Abcam).

MNs in the grey matter of the ventral horns were quantified as previously described [20]. MNs with diameters >25 μm and <25 μm and

polygonal shape were counted using a Leica DMD 108 microscope and Leica's LAS X image analysis software. Microglial and astroglial immunoreactivity was quantified using the ImageJ software and as previously described [1]. The Image J Sliding Paraboloid processing was applied to every image to minimize potential over-signaling.

Cytokines

Quantification of different cytokines (TNFα, IFNγ, IL1β, IL2, IL6, GM-CSF) in the CSF was performed using xMAP technology and a MAGPIX Luminex 200 platform (Thermo Fisher Scientific, Waltham, MA, USA) [1]. Briefly, after the incubation of a specific monoclonal antibody conjugated bead population with 50 μL of CSF samples for 1 h (room temperature), washed beads (color-coded beads of specific monoclonal antibodies) were incubated with detection antibody solution for 30 min, then with the streptavidin–phycoerythrin-conjugated solution (10 min). After washing, the beads were resuspended in the assay buffer, shaken for 1 min, and then read on the MAGPIX instrument. Results were analyzed with xPONENT 4.2® software (Luminex, Austin, TX, USA). The pro-inflammatory cytokines we analyzed have been found elevated in the CSF of ALS patients and murine models (see e.g. Refs. [21,22]). Thus, are representative as inflammation-related markers.

Samples of CSF were obtained following the methodology described in detail by Lim et al [1,23]. This procedure was performed in conditions of asepsis to avoid any bacterial contamination. Briefly, to collect the CSF, mice were first anesthetized with buprenorphine (0.1 mg/kg). Then, the hair at the back of the head of the mouse from above the eyes, between the ears to the bottom of the neck, was removed using clippers and depilatory cream. The head of the mouse was secured using an adapter. Using a dissecting microscope, scissors, and curved forceps, and by cutting through the skin and the layers of muscle, the base of the skull over the cisterna magna was exposed. The use of a micromanipulator and glass capillary-attached setup system allowed obtaining a total amount of ~10–15 μL of CSF in 10–30 min. The technique may cause, although rarely, some very minor bleeding which can be controlled using cotton buds and Cutoline Alum Hemostatic sticks; the area was cleaned for insertion of the glass capillary with distilled H_2O to avoid contamination of the sample. Microscopic analysis was routinely performed to detect blood contamination, and only samples with no blood contamination were used.

Isolation and culture of motor neurons, astrocytes and microglia

Isolation from mouse adult spinal cords and culture was based on previously described methodology [24]. Purity (>98 % in all cases) was checked by immunochemistry using the antibodies indicated above. No significant morphological differences were found comparing cells isolated from WT and $SOD1^{G93A}$ or FUS^{R521C} mice (see Additional File 1: Fig. S1). Compartmentation (cytosolic and mitochondrial compartments) of MNs was based on Obrador et al [1]. Isolated cells were cultured for 24 h before any addition or measurement.

Isolation and cultured of endothelial cells from the CNS

The procedure was based on previous methodology used to isolate sinusoidal endothelial cells from the liver. Tissue digestion was carried out at 37 °C by sequential perfusion (through the left ventricle) with type-E pronase (0.04 % in HBSS) plus collagenase A (0.08 % in HBSS) (Boehringer, Mannheim, Germany) (15 mL, 1 mL x min), and then with 0.1 % type-E pronase (10 mL, 1 mL x min) [25]. Then the medulla was surgically isolated, minced and stirred (10 min) in another solution containing pronase (0.04 %), collagenase (0.08 %) and DNAase (type I deoxyribonuclease; Merck) (0.0005 %). After enzymatic digestion, the solution was diluted in HBSS medium and the entire volume was filtered through sterile nylon gauze. The filtrate was centrifuged (10 min, 450 × *g*) at 4 °C and the same washing was repeated. The cell pellet was resuspended in 2.5 mL of HBSS and mixed with metrizamide previously dissolved in HBSS without Na^+. Endothelial cells were separated in a 17.5 % (w/v) metrizamide gradient. After centrifugation at 950 × *g* x 15 min (4 °C), the cells located in the upper gradient were separated, resuspended in DMEM, and seeded. Purity (>98 %) was checked by immunochemistry using an anti-RECA-1 monoclonal antibody (ab197727, abcam). Cultures of endothelial cells were established and maintained in pyrogen-free Dulbecco's modified Eagle's medium (DMEM; Gibco Labs., Grand Island, NY), pH 7.4, supplemented with 10 % fetal calf serum (Gibco), 10 mM HEPES, 40 mM $NaHCO_3$, 100 U/ml penicillin and 100 μg/ml streptomycin. Differential adhesion of endothelial cells to the collagen matrix and washing allows a complete elimination of other cell types (macrophages, lymphocytes, glia and neurons) from the culture flasks. No significant morphological differences were found comparing cells isolated from WT and $SOD1^{G93A}$ or FUS^{R521C} mice (see Additional File 1: Fig. S1). Isolated endothelial cells were cultured for 24 h before any addition or measurement.

Cell death analysis

Isolated MNs were incubated with Hoechst 33342 and propidium iodide [1], and analyzed using a Diaphot 300 fluorescence microscope (Nikon, Tokyo, Japan). Nuclei of viable, necrotic, and apoptotic cells were detected as blue round nuclei, pink round nuclei, and fragmented blue or pink nuclei, respectively. DNA strand breaks in apoptotic cells were assessed using the TUNEL labeling assay (Merck) and manufacturer's methodology.

ROS and NO generation

H_2O_2 and O_2^- generation assays followed previous methodology [26,27]. Cells were plated immediately after the isolation procedure, and measurements of H_2O_2 and NOx were performed 24 h after.

Briefly, the assay of H_2O_2 production was based on the H_2O_2-dependent oxidation of the homovanillic acid (3-methoxy-4-hydroxyphenylacetic acid) to a highly fluorescent dimer (2,2′-dihydroxydiphenyl-5,5′-diacetic acid), which is mediated by horseradish peroxidase. O_2^- generation was determined by flow cytometry using dihydroethidium (2 Ag/mL; Selleck Chemicals GmbH, Köln, Germany). For this purpose, cellular suspensions were diluted to 200,000 cell/mL. Analysis was done with a FACS Aria Fusion (BD, Franklin Lakes, NJ). Samples were acquired for 10,000 individual cells.

Nitrite and nitrate determination was based on the methodology of Braman and Hendrix [28]. Total NOx (NO_2^- plus NO_3^-) was assessed by monitoring NO evolution from a measured sample placed into a boiling VCl3/HCl solution (which reduces both NO_2^- and NO_3^- to NO). Quantitation was accomplished using a standard curve made up of known amounts of NO_2^- and NO_3^- [29].

Glutathione

Glutathione (GSH) was measured by HPLC/MS using a Quattro microTM triplequadrupole mass spectrometer (Micromass, Manchester, UK) equipped with a Shimadzu LC-10ADVP pump and SCL-10AVP controller system with an SIL-10ADVP autoinjector (Shimadzu Corp., Kyoto, Japan). Sample collection and processing were performed according to a published methodology.Briefly, cell samples were deproteinized with trichloroacetic acid (15 % final concentration) and rapid N-ethylmaleimide derivatization was performed to prevent GSH autooxidation. The acid-soluble fraction (approx. 200 μL) corresponds to

the supernatant obtained after centrifugation (15,000 × *g* × 5 min at 4 °C) [30,31].

Preparation of NO and peroxynitrate solutions

Thionitrobenzoic acid was used to characterize the stability of a NO solution obtained by bubbling a 50 mM HEPES-NaOH buffer (pH 7.4) with NO gas as previously described [32]. Levels of NO were measured as previously reported [33] using a Sievers NOA 280A chemiluminescence analyzer. Peroxynitrite was prepared from amyl nitrite and H_2O_2 following the methodology of Uppu and Pryor [34]. The concentration of $^{-}$OONO was measured spectrophotometrically (extinction coefficient of 1670 M^{-1} x cm^{-1} at 302 nm).

ATP

ATP was measured fluorimetrically following standard enzymic methods [35].

Caspase 3

This activity was measured by using a highly sensitive colorimetric substrate, N-acetyl-Asp-Glu-Val-Asp p-nitroanilide (Ac-DEVD-pNA) following manufacturer's instructions (CalBiochem, La Jolla, CA). Briefly, cells (5×10^5) were lysed in lysis buffer [50 mM HEPES (pH 7.4), 00 mM NaCl, 0.1 % (v/v) CHAPS, 1 mM dithiothreitol and 0.1 mM EDTA] on ice for 10 min, then centrifuged at 10,000 × *g* for 10 min (4 °C). Equal volumes of the supernatants were added to equal volumes of assay buffer [50 mM HEPES (pH 7.4), 100 mM NaCl, 0.1 % (v/v) CHAPS, 10 mM dithiothreitol, 0.1 mM EDTA, and 10 % glycerol] and incubated at 37 °C for 10 min. Then, freshly prepared Ac-DEVD-pNA (200 mM) was added to the mixture and A405 was monitored every 20 min for 3 h at room temperature. Cultures without cell lysates were used as controls. Enzyme activity was calculated as pmol/min using manufacturer's formulae.

Z-DEVD-FMK (Z-Asp-Glu-Val-Asp-fluoromethylketone; CalBiochem), dissolved in DMSO was used as an irreversible caspase-3 inhibitor.

Mitochondrial membrane potential

Quantitative determination of the mitochondrial membrane potential (MMP) was performed by the uptake of the radiolabeled lipophilic cation methyl triphenylphosphonium (TPMP), which enables small changes in potential to be determined [36]. Briefly, cells (2×10^6) were incubated at 37 °C for 60 min in 1 ml DMEM, supplemented as mentioned above but including 1 mM TPMP, 250 nCi 3HTPMP (Amersham, Bucks, UK), and 1 mM sodium tetraphenylboron. After incubation, the cells were pelleted by centrifugation (1000 × *g* for 5 min), 100 ml of the supernatant were removed, the pellet resuspended in 100 ml 10 % Triton X-100, and the radioactivity (disintegrations/min) was measured using a Tri-Carb Liquid Scintillation Counter from Perkin-Elmer (Waltham, MA). Non-specific TPMP binding was corrected as previously described [36]. Energization-dependent TPMP uptake was expressed as an accumulation ratio in units of [(TPMP/mg protein)/(TPMP/ml supernatant)] [37].

Oxygen consumption

It was measured in isolated cells using an oxygraph of OROBOROS Instruments (Innsbruck, Austria) and as previously described [18].

Mitophagy

The % of lysosomes that colocalize with mitochondria was quantified to analyze late-stage mitophagy [38]. MitoTracker™ Green FM (Thermo Fisher Scientific) and LysoTracker™ Red DND-99 (Life Technologies, Carlsbad, CA, USA) were used to stain mitochondria and lysosomes in live MNs, respectively. We followed manufacturer's instructions. For the mitotracker and lysotracker probes, the concentrations in the testing wells were 100 and 75 nM, respectively. In both cases, the incubation time was of 30 min at 37 °C. To take the images, we used a Leica TCS SP8 confocal microscope, a ×63 objective and a 2.5 zoom.

Enzyme activities and expression

To measure enzyme activities, cells were washed twice at 4 °C in Krebs-Henseleit bicarbonate medium (pH 7.4) without Ca^{2+} or Mg^{2+} added and containing 0.5 mM EGTA and then resuspended and homogenized in ice-cold lysis buffer [0.1 M PBS (pH 7.2) containing 1 mM phenylmethylsulfonyl fluoride, 10 mg/ml aprotinin, 10 mg/ml leupeptin, and 5 mg/ml pepstatin A (Sigma)] at a density of approx. 15×10^6 cells/ml. SOD1, SOD2, CAT and GPX activities were measured as previously described [26,39]. For NOS activity assay, 100 µl of supernatant was added to reaction mixture containing HEPES, 20.0 mmol/l (pH 7.4), 0.2 mM L-arginine (Sigma) and 2 mM NADPH (Sigma) in a total volume of 0.5 ml, and was then incubated under constant air bubbling (1 ml/min) at 37 °C for 120 min. The blank sample contained all reaction components except NADPH. NOS activity was calculated from the difference between samples and blank reading.

RT-PCR analysis was performed as previously described [1]. Briefly, 10^5 cells were mixed with lysis solution (Thermo Fisher Scientific) and incubated for 5 min at room temperature to lyse the cells and remove gDNA. Then, the stop solution (Thermo Fisher Scientific) was added and incubated for 2 min at room temperature. Samples were stored at −80 °C. Real time quantitation of each mRNA relative to glyceraldehyde-3-phosphate dehydrogenase mRNA was performed with a SYBR Green I assay and an iCycler detection system (Bio-Rad). Target cDNAs were amplified in separate tubes using as follows: 10 min at 95 °C and then 40 cycles of amplification (denaturation at 95 °C for 30 s and annealing and extension at 60 °C for 1 min per cycle). PCR master mix and AmpliTaq Gold DNA polymerase (Applied Biosystems) were added to the specific primers (Sigma Genosys), which were those previously reported for superoxide dismutases (SOD1 and SOD2), glutathione peroxidase (GPX), catalase (CAT) [1], inducible nitric oxide synthase (iNOS) and endothelial nitric oxide synthase (eNOS) [40]. The increase in fluorescence was measured in real time during the extension step. The threshold cycle (CT) was determined, and then the relative gene expression was expressed as follows: fold change $= 2^{-\Delta\,(\Delta CT)}$, where ΔC_T = C_T target - C_T glyceraldehyde-3-phosphate dehydrogenase, and $\Delta(\Delta C_T) = \Delta C_T$ treated - ΔC_T control.

Western blots

MNs were washed twice with phosphate-buffered saline, and the pellet was suspended in ice-cold homogenization buffer (2×10^6 cells per ml of buffer: 20 mM HEPES pH 7.5, 250 mM sucrose, 1 mM $MgCl_2$, 10 mM KCl, 1 mM EDTA, 1 mM EGTA, 1 mM dithiothreitol, 0.1 mM phenylmethylsulfonyl fluoride, and 10 mg leupeptin, aprotinin, and pepstatin A/ml). Proteins were quantified [41], separated by SDS-PAGE, transferred to nitrocellulose membranes, and subjected to western blotting. Anti-SOD1 (ab51254), anti-SOD2 (ab68155), anti-CAT (ab209211), anti-GPX1 (ab108427), anti-iNOS (ab178945), anti-eNOS (ab300071), anti-cytochrome C (ab133504) and anti-TLS/FUS [BLR023E] (ab243880) monoclonal antibodies were from abcam. Anti-SOD1 antibody (ALS mutant), clone MS785 (MABN834) was from Merck Millipore. Blocking was performed using 5 % BSA in TBST. The concentration of the different antibodies used was: 1:50,000 SOD1; 1:1000 SOD2; 1:2000 CAT; 1:200 GPX; 1:1000 iNOS and eNOS; 1:500 Cyt C; 1:1000 SOD1 (ALS mutant); 1:2000 TLS/FUS. The internal standard (5 µM/well) was from Thermo Scientific (ref. 26623). As a loading control, we used glyceraldehyde 3-phosphate dehydrogenase (GAPDH). Blots were developed using an anti-rabbit horseradish peroxidase-conjugated secondary antibody (1:2000) and enhanced chemiluminescence (ECL system; GE HealthCare Life Sciences, Uppsala, Sweden). Protein bands were

quantified using laser densitometry. To make the pooling of data from different immunoblots possible, the relative density of each band was normalized against the internal standard analyzed on each blot.

Hydroxyl free radical and peroxynitrite levels

Hydroxyl radicals were measured based on the methodology described by Deng et al [42]. The detection starts with the nitrite release from nitroimidazoles upon its specific reaction with ·OH radicals and subsequently nitrite quantification by Griess reagent, which forms a red substance. The color development is proportional to the amount of OH.

Peroxynitrite levels were measured using the Peroxynitrite Assay Kit of Abcam (ab233468). In this assay, a fluorescent probe specifically reacts with $^{-}$ONOO to generate a bright green fluorescent product.

For both assays cells were plated overnight in growth medium at 75,000 cells/well/100 µl for a 96-well plate.

Nitrosative stress biomarkers

The acid-soluble fractions (200 µl) obtained for GSH determination were added to 25 µl of 2.0 % ammonium sulfamate. To the mixtures were added 200 µl of 0.5 N HCl containing 0.25 % $HgCl_2$ and 5 %

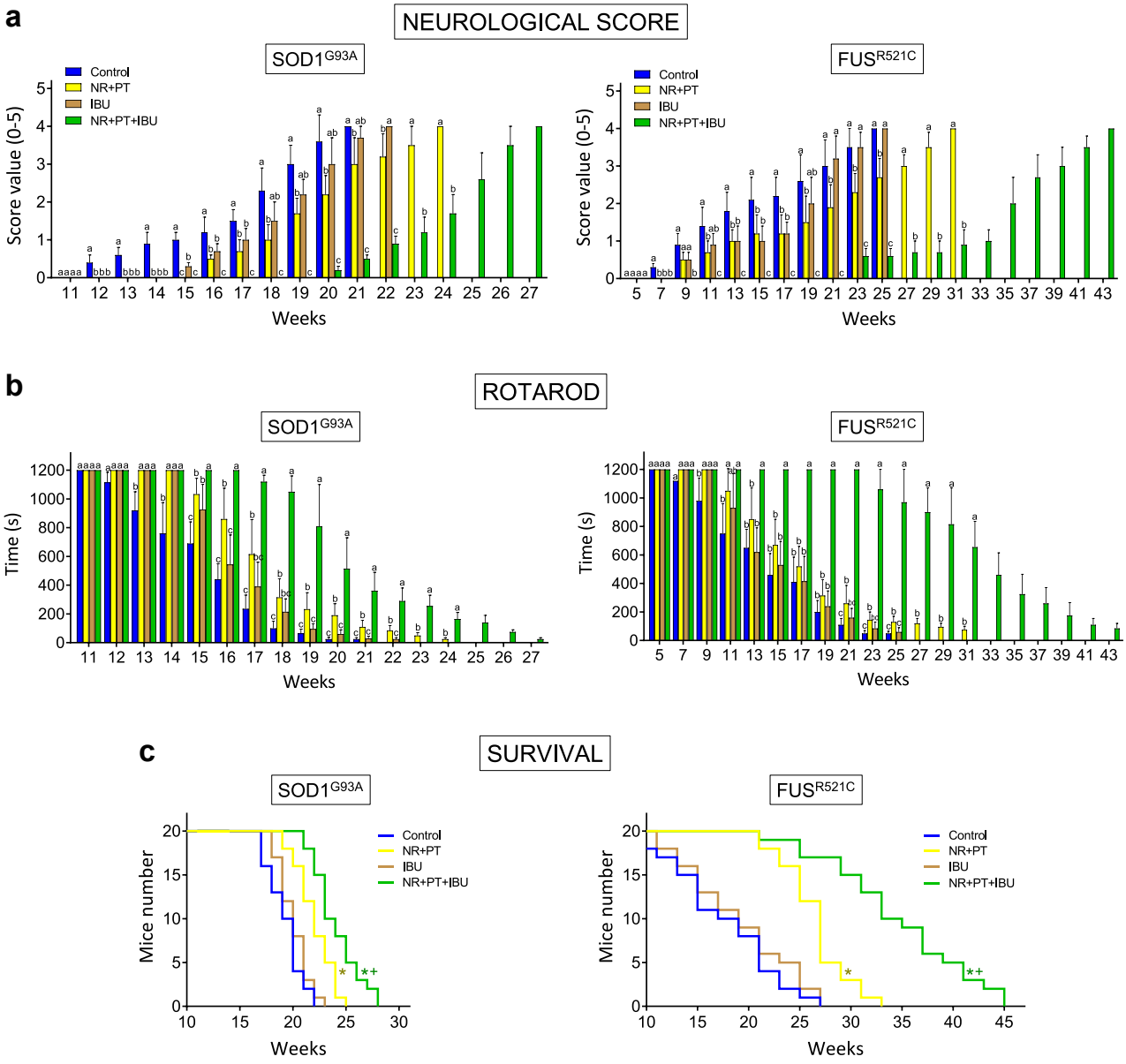

Fig. 1. NR + PT + IBU delay loss of functional performance and extend survival in SOD1^{G93A} and FUS^{R521C} mice. (a) Neurological score. (b) Rotarod test. (c) Survival. Treatment arms were as follows: physiological saline-treated transgenic mice (controls), SOD1 ^{G93A} or FUS^{R521C} mice treated with NR and PT, SOD1 ^{G93A} or FUS^{R521C} mice treated with IBU, and SOD1 ^{G93A} or FUS^{R521C} mice treated with NR, PT and IBU. The number of mice tested per week (tests a and b) was identical to that displayed in the survival experiments (c) for each experimental group. Both neuromotor tests (a, b) were performed twice a week. On the days of the week in which the animals were not scored, they were trained in the rotarod. Control experiments performed in WT mice ($n = 10$) rendered a neurological score of 0 and a performance time of 1200 s in the rotarod test in all cases. Taking into account the % of animals that died during disease progression, to assess the neurological score and the rotarod test, their number was increased so that n (15 mice) was approx. the same both at onset and at advanced progression. A one-way analysis of variance (ANOVA) was used to make comparisons among the different treatments at each time point. Different letters indicate statistical differences, $P < 0.05$ (a, b). Survival data were analyzed with Kaplan-Meier curves and LogRank (Mantel-Cox) test (*$P < 0.01$ comparing all groups versus controls; $^{+}P < 0.01$ comparing mice treated with NR + PT + IBU versus mice treated with NR + PT) (c).

sulfanilamide. Then, 250 µl of a 0.5 N HCl solution containing 0.25 % N-(1-naphthyl)ethylenediamide dihydrochloride were added to the mixtures. After incubation for 30 min at 25 °C, the amount of S-nitrosothiols (RSNO) was determined spectrophotometrically at 550 nm using S-nitrosoglutathione (GSNO) as a standard [43]. Fresh GSNO solution was obtained, before each experiment, by incubating equimolar GSH and sodium nitrite in acidified water at 0 °C as previously described [44]. GSNO concentration was determined spectrophotometrically at 335 nm ($\varepsilon = 992\ dm^3\ x\ mol^{-1}\ x\ cm^{-1}$) and at 545 nm ($\varepsilon = 15.9\ dm^3\ x\ mol^{-1}\ x\ cm^{-1}$). No significant decomposition of GSNO occurred during the assay procedures. Formation of 3-nitrotyrosine was measured using the ELISA kit from Cell Biolabs (San Diego, CA).

L-NAME administration

L-NAME (L-NG-nitro arginine methyl ester, Abmole Bioscience Inc., Houston, TX) was administered i.p. (20 mg/kg x day, starting on week 18; the administration of L-NAME was maintained until the death of the last mouse).

Statistical analysis

The G*Power 3.1.9.2 software was used to determine the sample size (ANOVA test, effect size = 0.21, $\alpha = 0.05$, $\beta = 0.80$ and 4 groups). Survival data were analyzed with Kaplan–Meier curves and LogRank (Mantel–Cox) test. Data are presented as mean values ± SD for the number of different experiments. Data were analyzed by one- or two-way analysis of variance (ANOVA) or unpaired t tests where appropriate (SPSS Statistics 29 for Windows; SPSS Inc., Chicago, IL). The homogeneity of the variances was analyzed by the Levene test. The null hypothesis was accepted for all the values of the tests in which the F value was nonsignificant at $n \geq 0.05$. The data for which the F value was significant was examined by Tukey's test at $P < 0.05$.

Results

NR, PT and IBU delay failure of neuromotor coordination and extends survival in murine ALS models

Neuromotor functions were studied in $SOD1^{G93A}$ and FUS^{R521C} mice using a standardized neurological score (designed to assess hind-limb function) (Fig. 1a) and the rotarod performance test (a measure of balance, coordination, physical condition and motor planning) (Fig. 1b). The onset of the symptomatology was around postnatal week 12 in $SOD1^{G93A}$ mice and postnatal week 7 in FUS^{R521C} mice. Both, the NR + PT treatment or IBU alone delayed the onset of the neurological symptomatology compared to control animals (Fig. 1a and b). However, that delay was more pronounced in mice treated with the triple combination (PT + NR + IBU) (Fig. 1a and b). These findings had a direct correlation with survival, which was significantly higher in mice treated with the triple combination compared to controls or treated with PT + NR or IBU (Fig. 1c).

We also assayed other currently used PDE inhibitors i.e. rolipram (a selective PDE4 inhibitor that may favor elimination of abnormal proteins via the proteasome), roflumilast (another PDE4 inhibitor with anti-inflammatory effects) and apremilast (a PDE4 inhibitor that can inhibit TNFα production by different cells). For this purpose we used the FDA conversion factor to transform pharmacological doses in humans [45] into equivalent doses in mice. However, none of them (one dose per day) was well tolerated by the ALS mice, which in less than 2 weeks of treatment developed gastrointestinal disorders (diarrhea, in mice treated with any of the 3 alternative PDE4 inhibitors), muscle spasms (mice treated with roflumilast) or signs of pain (mice treated with apremilast showed a hunched posture as the treatment advanced). This was not the case in ALS mice treated with NR + PT and/or IBU (see Additional File 1: Table S1).

NR, PT and IBU decrease spinal neuroinflammation and MN degeneration in murine ALS models

ALS progression associates with microgliosis and astrogliosis affecting the anterior horns of the medulla. Thus, immunohistopathological analysis of the medulla was performed to quantify microgliosis (immunohistochemical staining of Iba1) and astrogliosis (immunohistochemical staining of GFAP) in both rodent models. NR + PT or NR + PT + IBU reduced both types of neuroinflammation-associated gliosis (Fig. 2a and b). But only in the case of microgliosis (Fig. 2a), the triple combination was found significantly more effective than NR + PT. As an example, microscopic images are shown comparing thoracic spinal cord sections obtained from controls and mice treated with the triple combination (Fig. 2a and b).

At week 18 (Fig. 2c), the number of MN cell bodies in the anterior horns of the thoracic spinal cord [assessed by staining with anti-ChAT antibodies] was better conserved in both murine models treated with PT + NR or PT + NR + IBU and was not significantly different from that found in wild-type (WT) mice. Histological evaluation [hematoxylin and eosin staining] of spinal cord samples revealed loss of MNs in control $SOD1^{G93A}$ and FUS^{R521C} mice treated with physiological saline (PS). MNs appeared better conserved in mice treated with NR + PT + IBU (Fig. 2c). Nevertheless, just the number or the morphology does not inform of whether these MNs are fully functional or suffer some damage(s).

Our next step was to study a possible correlation between neuroinflammation and molecular signaling. To this end, we measured a number of proinflammatory cytokines in CSF samples obtained from WT, $SOD1^{G93A}$ and FUS^{R521C} mice. As shown in Fig. 3, the levels of all measured cytokines increased in the CSF of control $SOD1^{G93A}$ and FUS^{R521C} mice treated with PS, as compared to WT mice. Treatment of $SOD1^{G93A}$ and FUS^{R521C} mice with NR + PT significantly decreased the levels of IFNγ and IL6, whereas treatment with IBU was particularly effective in decreasing the TNFα (Fig. 3). When groups treated with NR + PT and groups treated with NR + PT + IBU were compared, only the levels of TNFα were significantly different (Fig. 3). These data indicate that, in both ALS models, IBU specifically decreases the levels of TNFα (Fig. 3).

NR, PT and IBU protect MNs against proinflammatory cytokine-induced oxidative and nitrosative stress

Oxidative stress an inflammation are part of the ALS pathophysiology [11]. Studies on the interaction of metastatic and endothelial cells have shown that TNFα, IFNγ and IL1β are cytokines capable of inducing generation of ROS and reactive nitrogen species (RNS) [29]. Moreover, vascular endothelium-derived NO and H_2O_2 were found to be cytotoxic for metastatic cells [29]. Thus, we investigated possible links between oxidative/nitrosative stress and different cells present in the MN microenvironment. As shown in Fig. 4, TNFα, IFNγ and IL1β increase NO (expressed as NOx: NO_2^- plus NO_3^-) and H_2O_2 generation by MNs, astrocytes, microglia and endothelial cells isolated from $SOD1^{G93A}$ and FUS^{R521C} mice, compared to equivalent cells isolated from WT mice. Except in the case of astrocytes, this effect was particularly evident when all three cytokines were incubated together (Fig. 4), a condition that better reflects the *in vivo* situation (see Fig. 3). None of the other cytokines measured in the CSF (IL2, IL6, GM-CSF, Fig. 3) did affect H_2O_2 or NO generation in the tested cells (data not shown).

As shown in Table 1, generation of H_2O_2 and NO was also investigated in the different cell types isolated from control $SOD1^{G93A}$ and FUS^{R521C} mice and from $SOD1^{G93A}$ and FUS^{R521C} mice treated *in vivo* with NR + PT, IBU or NR + PT + IBU. Treatment with NR and PT significantly decreased cytokine (TNFα, IFNγ and IL1β)-induced H_2O_2 and NO generation in all cell types, the exceptions being H_2O_2 in FUS^{R521C} astrocytes and NO in $SOD1^{G93A}$ astrocytes (Table 1). IBU decreased H_2O_2 generation in microglia and endothelial cells (Table 1). Whereas treatment with NR, PT and IBU further decreased H_2O_2 and NO

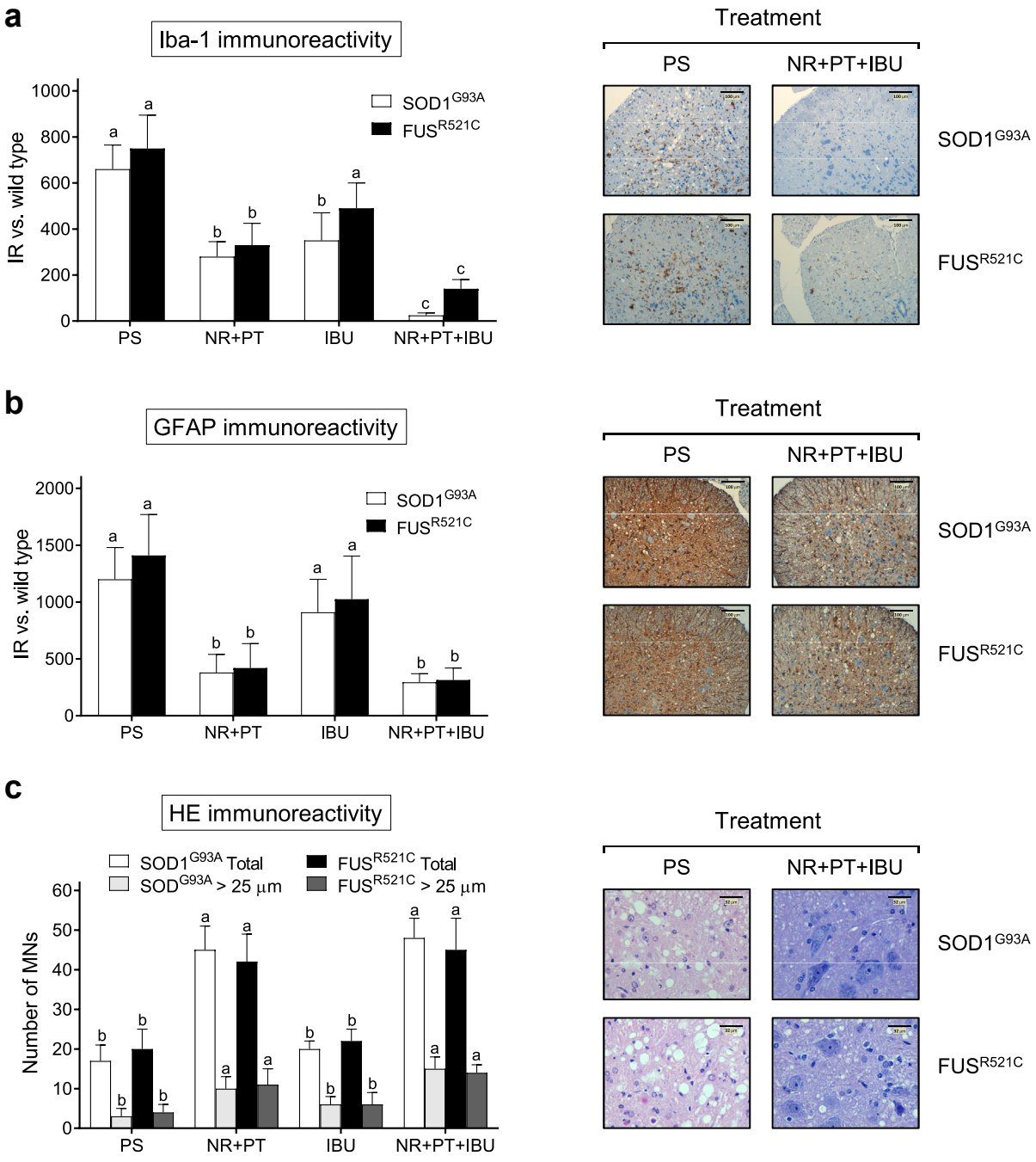

Fig. 2. NR + PT + IBU reduces motor neuron degeneration and neuroinflammation in the medulla. (a) Iba1 staining and immunoreactivity. (b) GFAP staining and immunoreactivity. (c) Number of MNs/section and HE staining. Tissue samples were obtained (at postnatal week 18/advanced state of progression) from SOD1 ^{G93A} and FUS^{R521C} 1C mice (see Fig. 1). Mice were treated with physiological saline (PS), NR + PT, IBU or NR + PT + IBU as in Fig. 1. All the mice were subjected to the tests and training indicated in Fig. 1. Representative images of microglia (Iba1) staining (a), astroglia (GFAP) staining (b) and hematoxylin and eosin staining (c) of the anterior horns of the thoracic spinal cord are shown, comparing mice treated with PS or NR + PT + IBU. a, b Glia quantification (IR, immunoreactivity). Reactive glia is quantified based on the immunostaining signal (arbitrary units), where the data obtained with the different treatments in ALS mice are subtracted from the data obtained in WT mice treated with PS. A one-way analysis of variance (ANOVA) was used to make comparisons among the different treatments. Different letters indicate statistical differences, $P < 0.05$ (a and b, $n = 7$; c, $n = 14$).

generation by microglia and endothelial cells, as compared with NR + PT treatment (Table 1). The generation of H_2O_2 and NO was more potent in microglia and endothelial cells than in MNs and astrocytes (Table 1). Thus, we focused our next experiments in microglia and endothelial cells, where we measured a battery of enzyme activities directly related with H_2O_2 and NO metabolism. As shown in Additional File 1: Table S1, as compared to WT mice, SOD1, SOD2, CAT and NOS activities increase in microglia and endothelial cells isolated from SOD1^{G93A} and FUS^{R521C} mice. Treatment with NR + PT + IBU significantly decreased SOD1 and NOS activities in both cell types, and SOD2 in the microglia (Additional File 1: Table S1). These changes in enzyme activities reflect the changes in H_2O_2 and NO generation described in Table 1, and correlate with changes measured in enzyme expression (Additional File 1: Fig. S2) and enzyme levels (Additional File 1: Fig. S3). Taken together, these results

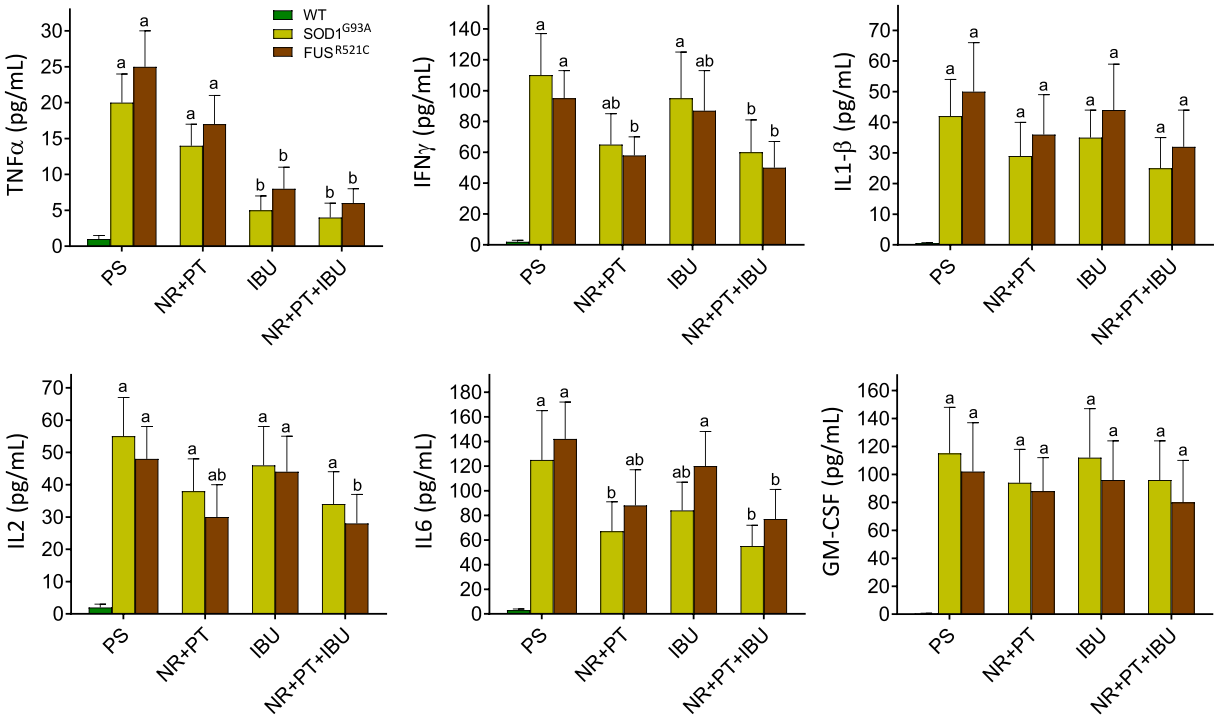

Fig. 3. Levels of proinflammatory cytokines in the cerebrospinal fluid of WT, SOD1^{G93A} and FUS^{R521C} mice. The CSF was obtained from ALS mice at week 18. Cytokines were measured as described under Methods. All mice were subjected to the tests and training indicated in Fig. 1. Mice were treated with PS, NR + PT, IBU or NR + PT + IBU as in Fig. 1A one-way analysis of variance (ANOVA) was used to make comparisons among the different treatments. Different letters indicate statistical differences, $P < 0.05$ ($n = 7$ in all cases).

demonstrate that specific proinflammatory cytokines can promote oxidative and nitrosative stress in the MN microenvironment.

Effect of the *in vivo* treatment with NR, PT and/or IBU. Cells were isolated from mice at week 18 of progression. Cytokines were incubated at the concentrations and time period indicated in Fig. 4. Mice were treated with NR, PT and/or IBU as in Fig. 1. Values are means ± SD of four to five different experiments. A one-way analysis of variance (ANOVA) was used to make comparisons among the different treatments. Different letters indicate statistical differences, $P < 0.05$.

Cytotoxicity by oxygen- and nitrogen-derived reactive species on MNs

The mechanism by which H_2O_2 and NO may induce MN cytotoxicity was further investigated in isolated MNs exposed to pathophysiological concentrations of these stress promoters. The concentrations selected for H_2O_2 and NO were based on the amounts generated together by the different cells (Table 1, controls, cells isolated at day 18 of *in vivo* progression). As shown in Table 2, H_2O_2 or NO cause a very low cytotoxicity (<10 %), in both models, compared with the basal medium-treated MNs. However, when H_2O_2 and NO were added together, we observed a much higher increase in MN cytotoxicity (approx. 40 % above controls) (Table 2). Moreover, –OONO also showed much higher cytotoxicity than H_2O_2 or NO alone (Table 2), which is remarkable and suggests that it is the combination of H_2O_2 and NO which probably causes greater cytotoxicity in the MNs. Incubation of the MNs in the presence of NO and SOD, which removes $O_2^{\cdot-}$ anions released to the extracellular medium and increases H_2O_2 levels, caused more cytotoxicity than NO alone (Table 2). We also used EGTA to remove metal ions present in the culture medium and found that H_2O_2- and NO-induced cytotoxicity decreased to values close to those found in the presence of NO alone (Table 2). Moreover, addition of H_2O_2, NO and $FeCl_3$ to EGTA-pretreated cells again increased MN cytotoxicity to values close to those induced by H_2O_2 and NO (Table 2). Ebselen, a synthetic organoselenium drug that mimics the GPX activity, and thus lowers H_2O_2 levels [46], also decreased the H_2O_2- and NO-induced MN cytotoxicity (Table 2). Taken together, these results suggest a trace metal-catalyzed process within a mechanism where different reactions may take place, i.e. (but not limited to) NO + H_2O_2, which generates NO_2^- + $^{\cdot}OH$ + H^+ via a Fenton reaction; Fe(III) + NO + H_2O_2, which generates Fe(II) + $^{-}OONO$ + $2H^+$; $^{\cdot}OH$ + H_2O_2, which generates $^{\cdot}OOH$ + H_2O; or $^{\cdot}OOH$ + NO, which generates $^{-}OONO$ + H^+. Mechanisms that produce potent oxidants, such as $^{\cdot}OH$ and $^{-}OONO$, could be mainly responsible of the NO- and H_2O_2-induced MN death.

In order to prove this hypothesis, we also measured generation of $^{\cdot}OH$ and $^{-}OONO$ by microglia and endothelial cells, the cell types that generate higher levels of H_2O_2 and NO (Table 1). As shown in Additional File 1: Fig. S4, microglia and endothelial cells isolated from the ALS mice generate higher levels of $^{\cdot}OH$ and $^{-}OONO$ than their normal counterparts isolated from WT mice. Moreover, the effect of NR + PT or NR + PT + IBU on these reactive species (Additional File 1: Fig. S4) correlates with that reported for H_2O_2 and NO in Table 1.

Oxidative and nitrosative stress trigger MN death

As a proof of concept, the effect of pathophysiological concentrations of H_2O_2 and NO on MN viability was measured in MN isolated from FUS^{R521C} mice. As shown in Fig. 5a, oxidative/nitrosative stress-induced MN death is mainly apoptotic. In agreement with the findings displayed in Table 2, the number of dead MNs was higher in the presence of H_2O_2 and NO (Fig. 5a). This correlated with molecular changes associated to the mitochondria-dependent activation of apoptotic cell death, including a decrease in mitochondrial membrane potential, GSH and ATP; an increase in mitochondrial O_2 consumption; and an increase in cytosolic caspase 3 activity and cytochrome C levels (Fig. 5b) (original uncropped gels for Fig. 5b, as well as for Fig. S3, are shown in Fig. S6). Furthermore, different studies have demonstrated that loss of autophagy/mitophagy can lead to an increase in ROS generation, which can, in turn, activate immune signalling pathways and the release of inflammatory cytokines [47]. We found that mitophagy (based on the percentage of lysosomes

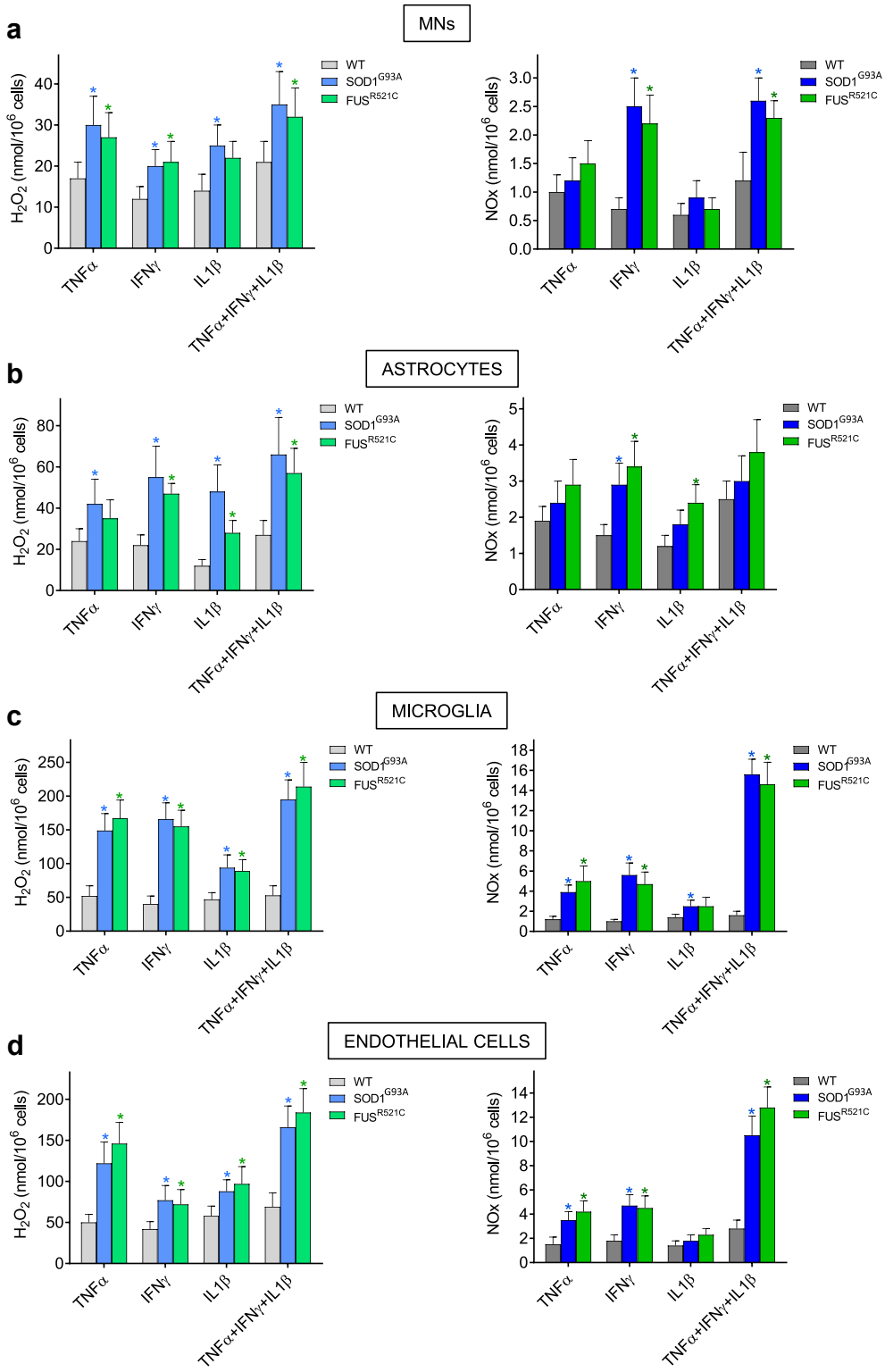

Fig. 4. *In vitro* production of H_2O_2 and NO by cytokine-activated MNs (a), astrocytes (b), microglia (c) and endothelial cells (d). Cells were isolated from mice at week 18 of progression and plated immediately after. Isolated cells were incubated x 24 h before addition of the cytokines. The concentrations used for each cytokine were selected based on the results obtained in Fig. 3. All cytokines were recombinant murine (rmTNFα and rmIFNγ were obtained from Merck; and rmIL1β from Sino Biological Europe GmbH, Eschborn, Germany). H_2O_2 and NOx were measured 6 h after adding the cytokines to the culture flasks. Data represent the total amount of NOx and H_2O_2 that accumulated in the medium during the indicated 6 h-period. rmTNFα concentrations in the culture medium were 1 (cells isolated from WT mice) or 25 pg/ml (cells isolated from $SOD1^{G93A}$ or FUS^{R521C} mice). rmIFNγ concentrations in the culture medium were 2 (cells isolated from WT mice) or 100 pg/mL (cells isolated from $SOD1^{G93A}$ or FUS^{R521C} mice). rmIL1β concentrations in the culture medium were 0.5 (cells isolated from WT mice) or 50 pg/ml (cells isolated from $SOD1^{G93A}$ or FUS^{R521C} mice). Values are means ± SD of five to six different experiments. *$P < 0.05$ (*t*-test) comparing cells isolated from $SOD1^{G93A}$ or FUS^{R521C} mice versus cells isolated from WT mice.

Table 1
Cytokine (rmTNFα, rmIFNγ and rmIL1β)-induced H_2O_2 and NO production by MNs, astrocytes, microglia and endothelial cells.

	Control		NR + PT		IBU		NR + PT + IBU	
	(nmol/10^6 cells)		(nmol/10^6 cells)		(nmol/10^6 cells)		(nmol/10^6 cells)	
	$SOD1^{G93A}$	FUS^{R521C}	$SOD1^{G93A}$	FUS^{R521C}	$SOD1^{G93A}$	FUS^{R521C}	$SOD1^{G93A}$	FUS^{R521C}
MNs								
H_2O_2	35 ± 8^a	32 ± 7^a	18 ± 4^b	16 ± 4^b	25 ± 5^{ab}	24 ± 6^{ab}	12 ± 3^b	10 ± 2^b
NOx	2.6 ± 0.4^a	2.3 ± 0.3^a	1.5 ± 0.4^b	1.2 ± 0.3^b	2.5 ± 0.7^a	2.4 ± 0.8^a	1.4 ± 0.4^b	1.3 ± 0.4^b
Astrocytes								
H_2O_2	66 ± 18^a	57 ± 12^a	39 ± 8^b	42 ± 11^a	50 ± 17^{ab}	51 ± 18^a	30 ± 7^b	28 ± 6^b
NOx	3.0 ± 0.7^a	3.8 ± 0.9^a	2.0 ± 0.5^b	2.4 ± 0.5^b	2.8 ± 0.8^a	3.6 ± 1.0^{ab}	1.8 ± 0.3^b	2.0 ± 0.5^b
Microglia								
H_2O_2	195 ± 29^a	214 ± 36^a	110 ± 18^b	126 ± 23^b	137 ± 21^b	156 ± 27^{ab}	65 ± 20^c	74 ± 16^c
NOx	15.6 ± 1.5^a	14.6 ± 2.2^a	8.5 ± 1.2^b	7.4 ± 0.9^b	14.2 ± 1.3^a	12.7 ± 2.0^a	5.7 ± 1.2^b	5.0 ± 1.1^b
Endothelial cells								
H_2O_2	166 ± 26^a	184 ± 29^a	84 ± 17^b	96 ± 17^{bc}	114 ± 19^b	129 ± 19^b	43 ± 15^c	55 ± 18^c
NOx	10.5 ± 1.6^a	12.8 ± 1.7^a	8.6 ± 1.3^a	9.2 ± 1.5^a	9.6 ± 1.6^a	11.5 ± 1.7^a	5.4 ± 1.2^b	5.7 ± 1.5^b

[a]: highest mean value.
[b]: significantly different from "b".
[ab]: values that are not significantly different from either "a" or "b".
[c]: lowest mean value.

Table 2
MN cytotoxicity of nitrogen- and/or oxygen derived reactive species.

Additions	MN cytotoxicity (%)	
	$SOD1^{G93A}$	**FUS^{R521C}**
Basal medium	2 ± 1^d	1 ± 0.5^d
NO	10 ± 4^c	8 ± 3^c
H_2O_2	7 ± 3^{cd}	10 ± 4^c
NO + H_2O_2	42 ± 7^a	38 ± 8^a
$^-$OONO	28 ± 5^b	30 ± 7^a
NO + SOD	25 ± 6^b	28 ± 6^{ab}
NO + H_2O_2 + EGTA	14 ± 4^c	10 ± 3^c
NO + H_2O_2 + EGTA + $FeCl_3$	50 ± 7^a	45 ± 10^a
NO + H_2O_2 + ebselen	15 ± 3^c	17 ± 4^{bc}

MNs were cultured for 24 h before any addition. NO (10 μM), H_2O_2 (100 μM), superoxide dismutase (SOD; 100 units/mL, Merck), $^-$OONO (10 μM), EGTA (0.5 mM), or ebselen (10 μM, Merck) were added at 24 h of culture. $FeCl_3$ (1 mM) was added 5 min after EGTA addition. Cytotoxicity is expressed as the % of MNs that lost viability within a 3-h period of incubation. Data are means ± S.D. of seven different experiments. A one-way analysis of variance (ANOVA) was used to make comparisons among the different treatments. Different letters indicate statistical differences, $P < 0.05$.

that colocalize with mitochondria) was also increased, as compared to controls, in MNs isolated from NR + PT- or NR + PT + IBU-treated FUS^{R521C} mice; and was even higher in mice treated with the triple combination versus those treated with NR + PT (Fig. 5c). Thus, suggesting that lysosomal elimination of damaged mitochondria is promoted by the protective treatments.

In vivo treatment with a NOS inhibitor increases survival in ALS mice

To further investigate the direct involvement of NO in ALS progression and on the mechanism that leads to MN damage, we tested the *in vivo* administration of a specific NOS activity inhibitor on $SOD1^{G93A}$ and FUS^{R521C} mice. As shown in Fig. 6a, *in vivo* treatment with L-NG-nitro arginine methyl ester (L-NAME) (starting at week 18; advanced state of progression) decreased levels of nitrosative stress-related biomarkers (nitrosothiols and nitrotyrosine). L-NAME treatment also decreased NOx (NO_2^- plus NO_3^-) generation by MNs, astrocytes, microglia and endothelial cells (Fig. 6b). *In vivo* treatment with L-NAME, administered to ALS mice, also increased survival as compared to controls (Fig. 6c). We did not assay the treatment for a longer period of time (e.g. starting earlier) to avoid potential L-NAME-induced systemic toxicities, i.e. hypertension [48], hepatic and intestinal toxicity [49] or nephrotoxicity [50]. Taken together, these results (see also Table 2) indicate that NO, and consequently mixed nitrogen- and oxygen-derived reactive species, cytokines and neuroinflammation are involved in the mechanism that leads to the damage of MNs.

In vivo treatment with NR and PT or L-NAME reduces the levels of mutant FUS protein

A further question we investigated was whether the levels of mutant SOD1 and FUS proteins could be also altered by the treatments displayed above. We analyzed the levels of these proteins by western blots in control mice (treated with physiological saline) and in mice treated with NR + PT, IBU, NR + PT + IBU and L-NAME following the treatment protocols (described above) in each case. Treated mice were at an advanced state of progression, so that the results are directly comparable with the experiments described in this manuscript. As shown in Additional File 1: Fig. S5, none of the experimental treatments varied the intracellular levels of mutant SOD1. This suggesting that the effectiveness of the treatments in $SOD1^{G93A}$ mice affects the pathophysiological consequences of the mutation and not its genetic causes. However, the case of FUS mice was found different. Treatment with NR + PT or with L-NAME decreased the accumulation of the mutant protein within the MNs. This fact can be interpreted in different ways. Treatments interfere in the pathophysiological consequences of the mutation (as in $SOD1^{G93A}$ mice). But, alternatively, alterations in the levels of cytokines, ROS or NO may also affect the transcription [via the C/EBP homologous protein (CHOP) transcription factor]-expression mechanisms [51] leading to the synthesis of the mutant protein; and/or the mutant FUS protein is being eliminated in a more efficient way (e.g. through the ubiquitin-proteasome system) [52].

Discussion

Neuroinflammation affects motor regions of the CNS in ALS [3]. During progression of the disease, in the anterior horns of the medulla microglia and astrocytes develop a phenotypic transition, proliferate, and secrete proinflammatory cytokines [53]. Consequently, it is assumed that chronic inflammation exacerbates MN degeneration [3], and that oxidative stress is linked to the damage of MNs.

NAD^+ is a coenzyme in redox reactions, a donor of ADP-ribose for ADP-ribosylation reactions, a precursor of cyclic ADP-ribose, and a substrate for sirtuins that use the cofactor to remove acetyl groups from proteins. Sirtuins link NAD^+ levels to mitochondrial function, dynamics and biogenesis, and to cellular antioxidant defenses (see e.g. Ref. [54]. Mitochondria have shown to be an early target in ALS pathophysiology

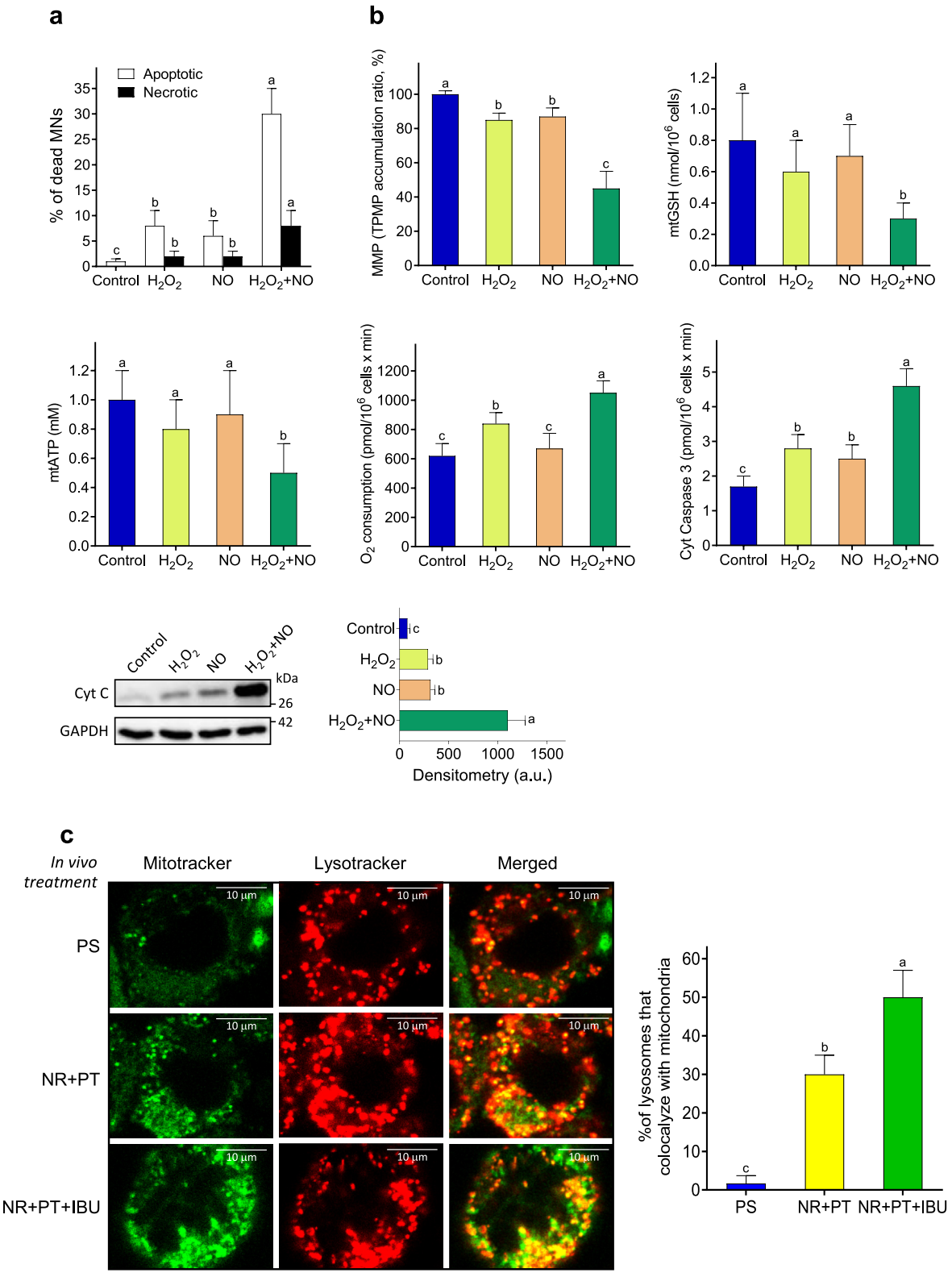

Fig. 5. H_2O_2- and NO-induced activation of MN death. MNs were isolated from FUS^{R521C} mice (week 18). For the analysis of cell death (a) and the tests related to the molecular activation of apoptosis (b), cells were treated as indicated in Table 2. Data are means ± SD of 4-5 different experiments. (c) Mitophagy analyses using lysosomal- and mitochondrial specific fluorescent dyes in live MNs. The graph corresponds to the average percentage of lysotracker puncta that colocalize with mitochondria (mean values ± SD for 4–5 different mice per experimental condition). A one-way analysis of variance (ANOVA) was used to make comparisons among the different treatments. Different letters indicate statistical differences, $P < 0.05$.

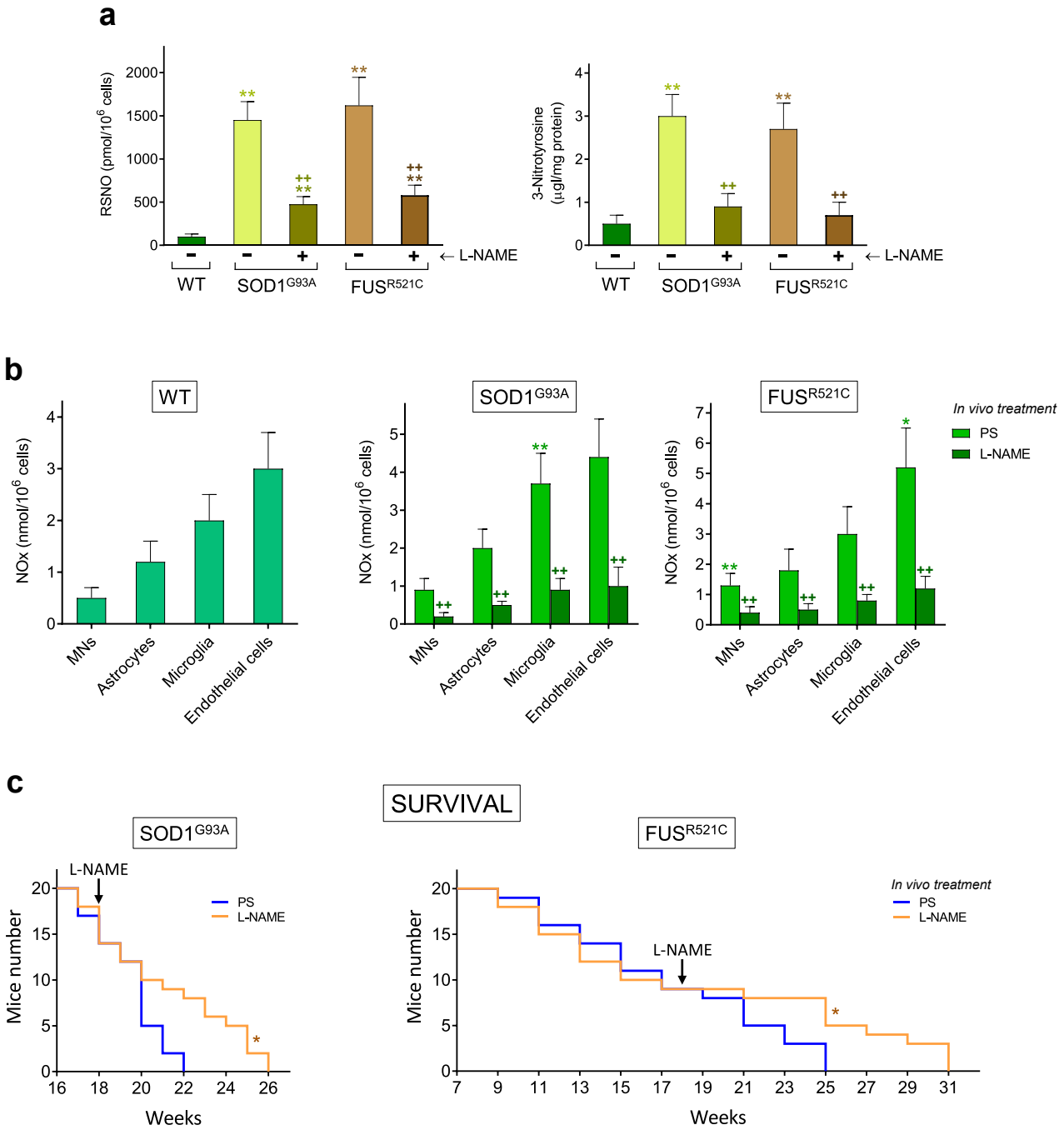

Fig. 6. Treatment with L-NAME decreases NO generation and increases survival in ALS mice. (a) Nitrosative stress biomarkers were measured in MNs isolated from WT mice and from ALS mice (treated with PS or with L-NAME). L-NAME was administered i.p. (as indicated under Methods and until the death of the last mouse). $^{*}P < 0.05$, $^{**}P < 0.01$ comparing ALS versus WT mice: $^{++}P < 0.01$ comparing ALS mice treated with L-NAME versus control ALS mice treated with PS ($n = 4$–5). (b) NOx generated (NO_2^- plus NO_3^-, see under Methods), during 3 h of *in vitro* incubation, by MNs, astrocytes, microglia and endothelial cells (isolated from WT and ALS mice). $^{*}P < 0.05$, $^{**}P < 0.01$ comparing cells isolated from ALS mice versus cells isolated from WT mice; $^{++}P < 0.01$ comparing cells isolated from L-NAME-treated ALS mice versus cells isolated from control ALS mice treated with PS ($n = 4$–5, *t*-test). (c) Mice survival. Data were analyzed with Kaplan-Meier curves and LogRank (Mantel-Cox) test ($^{*}P < 0.01$ comparing L-NAME-treated mice versus controls treated with PS, $n = 20$ as in Fig. 1).

progression. In fact, disruption of their axonal transport, excessive generation of ROS, disruption of the mitochondrial structure, dynamics, mitophagy, energy production, calcium buffering and apoptotic triggering have all been directly involved in disease pathogenesis and extensively reported in ALS patients and in different animal models (see e.g. Ref. [11]).

Our recent results show that treatment with NR and PT extends survival SOD1^{G93A} mice [1]. NR and PT increase the Nrf2-dependent antioxidant defenses and the activity of sirtuins 1 and 3 in MNs of SOD1^{G93A} mice [1]. PT favors overexpression of sirtuin 1 and nuclear translocation of Nrf2, whereas NR provides NAD^+ for the PARP-1 and sirtuin catalyzed reactions [1]. Thus, NR + PT decreases oxidative stress and, thereby, may help to reduce the release of pro-apoptotic signals from mitochondria (a complex mechanism involving many other interrelated factors such as Ca^{2+} accumulation, mitochondrial DNA damage, changes in the mitochondrial membrane potential, or alterations in the balance of

pro-apoptotic/apoptotic proteins). Therefore, plausibly, a combined strategy targeting neuroinflammation and oxidative stress could render beneficial effects. Here we show that PT + NR + IBU, as compared to the treatment with NR + PT, further delays progression of the neuromotor damage and increases survival in two models of ALS (Fig. 1). These effects associated with reduced neuroinflammation (Fig. 2a and b) and a decrease in the levels of different proinflammatory cytokines in the CSF (Fig. 3). Studies by Zhao et al. [55] in primary MN cultures showed that microglia, activated by lipopolysaccharide or IgG immune complexes, induced a MN injury which was prevented by a microglial inducible NOS (iNOS) inhibitor as well as by CAT or GSH. Pehar et al. [56] observed that cultured embryonic MNs expressing p75(NTR) were not vulnerable to the nerve growth factor unless they were exposed to an exogenous flux of NO. Thus, suggesting that NO plays a role in the pathophysiological cascade of ALS. We found that different cytokines (i.e. TNFα, IFNγ and IL1β) increase H_2O_2 and NO generation by MNs, astrocytes, microglia and endothelial cells isolated from ALS mice (Fig. 4). NR + PT decreased H_2O_2 and NO generation in all these cells (Table 1). PT alone has been shown to reduce microglial NO production when stimulated by LPS without directly scavenging NO radicals [57]. A mechanism that appears to work via inhibition of NO and TNFα production in microglia by blocking IkBα phosphorylation [58]. Here we present evidence showing that the combined treatments, either NR + PT or NR + PT + IBU, cause a significant decrease in the NO production in all the cells tested (Table 1). IBU was particularly efficacious in decreasing levels of TNFα in the CSF and the generation of H_2O_2 by microglia and endothelial cells (Table 1). Unexpectedly, exposure of MNs to pathophysiological concentrations of H_2O_2 or NO caused minimal cytotoxicity (Table 2). However, MN cytotoxicity was highly increased in the presence of H_2O_2 and NO, presumably due to the formation of potent oxidants, i.e. $^{\cdot}OH$ and $^{-}OONO$ radicals (Additional File 1: Fig. S4), via a trace metal-dependent process (Table 2).

These findings indicate that it is the proinflammatory cytokine-induced oxidative and nitrosative stress that is highly harmful to MNs, and that different cells in the microenvironment of the anterior horns are involved including microglia, astrocytes, endothelial cells and, likely, infiltrated immune cells. It is noteworthy to highlight that microglia displays different phenotypes during ALS progression, from surveillant in early stages to activated states M1 and M2, characterized by the expression of respectively harmful and protective genes in later phases of the disease [59]. Although our methodology to isolate microglial cells does not differentiate between the different phenotypes, it is evident that microglia isolated at week 18 of progression release pro-inflammatory cytokines (Fig. 4c).

The concentrations of H_2O_2 and NO used in the experiments displayed in Table 2 derive from the amounts generated by different cells present in the anterior horns (Table 1, control cells isolated at day 18 of *in vivo* progression). Thus, these concentrations may be considered as maximum pathophysiological levels. Nevertheless, the complex tissue architecture, the blood/lymphatic/CSF flows, as well as other regulatory molecules, are also important limiting factors not present in the *in vitro* experimental setting. Therefore, it is plausible to expect that, *in vivo*, MNs will be exposed to lower levels of H_2O_2 and NO. Possibly, since ALS often progresses in sporadic outbreaks, exposure of MNs to toxic levels of ROS and RNS may not be constant. All facts which would better fit with a more progressive deterioration. Moreover, cell and neuroanatomical region specificity of degeneration in ALS is often accompanied by the aberrant misfolding, aggregation, and deposition of specific proteins, such as SOD1 [60], TARDNA-binding protein of 43 kDa (TDP-43) [61], or fused in sarcoma (FUS) [62]. Both, ROS and RNS can favor abnormal protein aggregation (see Refs. [63,64]).

Furthermore, a recent case-control study concluded that occupational exposure to particulate matter, volatile organic compounds, metals, pesticides, and combustion and diesel exhaust was associated with an increased ALS risk. This study involved 381 ALS and 272 control participants [65]. A systematic review that analyzed 50 studies dealing with the relationship between metals and ALS found only 3 studies that suggested such an association, but only with selenium. No link with lead, mercury, aluminum, cadmium, chromium, or manganese was observed [66]. Nevertheless, a recent meta-analysis reported unusual changes in several indicators representing iron status [67]. This study showed that serum ferritin levels were higher and transferrin levels were lower in ALS patients compared with healthy controls. Transferrin's ability to reduce the levels of free iron in circulation suggests that this protein could have a protective effect for neurons in the context of ALS. Thus, suggesting a link with the mechanism described above. Therefore, to control the levels of free metals in blood and their dietetic or accidental intake could be important in ALS.

IBU, an anti-inflammatory drug firstly developed to treat asthma, is a cyclic nucleotide PDE inhibitor, which mainly acts by increasing the amount of cAMP and cGMP, while downregulating the pro-inflammatory factors, such as TNFα, macrophage migration inhibitory factor (MIF) and Toll-like receptor 4 (TLR-4) [68,69]. Pharmacologically, IBU may provide significantly prolonged time-to-first relapse and attenuate brain volume shrinkage in patients with relapsing-remitting and/or secondary progressive multiple sclerosis [70]. Experimentally, reduced neuroinflammation, inhibition of apoptosis, or interactions at the ubiquitin-proteasome pathway, have been suggested as possible neuroprotective mechanisms induced by IBU [70–72]. The IBU-induced decrease of TNFα levels in the CSF (Fig. 3) also suggests a decrease in the generation of mitochondria-derived ROS (Table 1, see also [1]). Hennet et al. [73] and Goossens et al. [74] first reported that TNFα promotes ROS formation by mitochondria. Consequently, IBU-induced decrease of TNFα levels suggests a potential decrease of mitochondria-derived ROS. Therefore, IBU appeared as a good candidate to complement the benefits elicited by NR and PT. Nevertheless, although NR and PT treatment did not show any significant toxicity in the $SOD1^{G93A}$ model [1] or in ALS patients [2], IBU treatment may face side effects-related limitations, such as e.g. gastrointestinal or skin disorders [75]. The dose of IBU used *in vivo* in this work (12 mg/kg x day, single dose), based on the accepted FDA conversion factor, is equivalent to approx. 0.97 mg/kg x day in humans. Hence, a patient of approx. 70 kg body weight should be taking a daily oral dose of 67.9 mg, and IBU shows an excellent safety profile at 60 mg/day [75].

In conclusion, our results show that the association of IBU with NR and PT can improve the protection of MNs in ALS. This combination decreases the proinflammatory cytokine-induced oxidative and nitrosative stress, which is highly harmful to MNs. Further, this study presents direct evidence that potent oxidants, such as $^{\cdot}OH$ and $^{-}OONO$, which can cause oxidation of lipids, protein and DNA, could be mainly responsible for this damage via a trace metal-catalyzed mechanism. The use of PT + NR + IBU and/or NOS inhibitors (which are following clinical trials, see NCT04562831, NCT05095571 and NCT04057898 in clinicaltrials.gov and [76]) may represent a novel strategy for the treatment of ALS. The pathophysiology of ALS clearly involves a cascade of molecular events and, as exemplified by our results, a judicious combination of several drugs may be more beneficial than the use of individual drugs. Moreover, the complex pathophysiology of the disease (as well as the negative results of many clinical trials), suggests that targeting patients early in their disease course may be critical.

The symptoms begin to be evident (measurable) after the death of a sufficient number of MNs where progressive damage is accumulating. The murine models of ALS are transgenic where, from the beginning, we know that the mutation will cause the development of neuromotor damage. And, we also know approximately when. This is not the case in ALS patients, where available treatments usually start (in the best case) after a pre-diagnosis, when the initial symptomatology is already evident. When we planned the experiments of a previous work [1], we observed that if treatment (NR + PT) began about 3 weeks before the onset of symptoms, survival was greater over time (an average time of approximately 1 week more in the case of $SOD1^{G93A}$ mice) comparatively to starting treatment right at the moment the symptoms begin. Weaning in

our mouse models is at 3 weeks after birth. So, we decided to begin the treatment 1 week after weaning (and we followed the same strategy in the present work). These facts exemplify the need to have early biomarkers that can indicate, in humans, the presence of a potential ALS-associated neuromotor disorder. This would allow treatment to be applied before clinical symptoms become evident. In practice, even before the appearance of symptoms, early treatment should be considered in people with known mutations associated with ALS etiology (familial ALS). Naturally, without reliable biomarkers, clinical decisions are much more complicated in cases of sporadic ALS.

Ethics approval and consent to participate

Not applicable.

Availability of data and materials

Data, materials and software information supporting the conclusions of this article are included within the article and its additional file. All raw data regarding these studies are available at the Figshare repository (https://figshare.com/s/4bcf46c7087a11b6150b).

Funding

This research was supported by grants from the Generalitat Valenciana (Spain) (AICO/2021/245) and from the University of Valencia (Spain) and Elysium Health Inc. (USA) (OTR2017-18255INVES and OTR2018-19337INVES).

Authors' contributions

R.L.B., P.M.M. and E.O.: animal treatments and motor coordination tests; R.L.B., R.S., M.O.C., P.M.M., R.W.D., J.M.E. and E.O.: measurement of cytokines, ROS, NO, and different cellular parameters; J.M.E.: pathology and cell death analysis; R.L.B. and P.M.M.: cell isolation and compartmentation; R.L.B. and M.O.C.: measurement of metabolites and enzyme activities; M.O.C. and P.M.M.: enzyme expression and western blots; R.S., E.O. and J.M.E.: statistics; J.M.E.: study design and supervision of all the experimental work; R.W.D., J.M.E. and E.O.: wrote the manuscript.

Declaration of competing interest

The authors declare the following financial interests/personal relationships which may be considered as potential competing interests: Jose M. Estrela reports financial support was provided by Elysium Health Inc. Elena Obrador reports financial support was provided by Government of Valencia. Ryan W. Dellinger reports a relationship with Elysium Health Inc. that includes: employment. Jose M. Estrela has patent #US2022/0160745A1 issued to Elysium Health Inc.

Acknowledgements

Not applicable.

Appendix A. Supplementary data

Supplementary data to this article can be found online at https://doi.org/10.1016/j.neurot.2023.10.011.

References

[1] Obrador E, Salvador R, Marchio P, López-Blanch R, Jihad-Jebbar A, Rivera P, et al. Nicotinamide riboside and pterostilbene cooperatively delay motor neuron failure in ALS SOD1G93A mice. Mol Neurobiol 2021;58:1345–71.
[2] de la Rubia JE, Drehmer E, Platero JL, Benlloch M, Caplliure-Llopis J, Villaron-Casales C, et al. Efficacy and tolerability of EH301 for amyotrophic lateral sclerosis: a randomized, double-blind, placebo-controlled human pilot study. Amyotroph Lateral Scler Front Degener 2019;20:115–22.
[3] Liu J, Wang F. Role of neuroinflammation in amyotrophic lateral sclerosis: cellular mechanisms and therapeutic implications. Front Immunol 2017;8:1005.
[4] D'Ambrosi N, Cozzolino M, Carrì MT. Neuroinflammation in amyotrophic lateral sclerosis: role of redox (dys)Regulation. Antioxid Redox Signal 2018;29:15–36.
[5] Pollari E, Goldsteins G, Bart G, Koistinaho J, Giniatullin R. The role of oxidative stress in degeneration of the neuromuscular junction in amyotrophic lateral sclerosis. Front Cell Neurosci 2014;8:131.
[6] Mittal M, Siddiqui MR, Tran K, Reddy SP, Malik AB. Reactive oxygen species in inflammation and tissue injury. Antioxid Redox Signal 2014;20:1126–67.
[7] Smith EF, Shaw PJ, De Vos KJ. The role of mitochondria in amyotrophic lateral sclerosis. Neurosci Lett 2019;710:132933.
[8] Wiedemann FR, Manfredi G, Mawrin C, Beal MF, Schon EA. Mitochondrial DNA and respiratory chain function in spinal cords of ALS patients. J Neurochem 2002;80:616–25.
[9] Ghiasi P, Hosseinkhani S, Noori A, Nafissi S, Khajeh K. Mitochondrial complex I deficiency and ATP/ADP ratio in lymphocytes of amyotrophic lateral sclerosis patients. Neurol Res 2012;34:297–303.
[10] Israelson A, Arbel N, Da Cruz S, Ilieva H, Yamanaka K, Shoshan-Barmatz V, et al. Misfolded mutant SOD1 directly inhibits VDAC1 conductance in a mouse model of inherited ALS. Neuron 2010;67:575–87.
[11] Obrador E, Salvador-Palmer R, López-Blanch R, Jihad-Jebbar A, Vallés SL, Estrela JM. The link between oxidative stress, redox status, bioenergetics and mitochondria in the pathophysiology of ALS. Int J Mol Sci 2021;22:6352.
[12] Evans CS, Holzbaur ELF. Autophagy and mitophagy in ALS. Neurobiol Dis 2019;122:35–40.
[13] Mizuno T, Kurotani T, Komatsu Y, Kawanokuchi J, Kato H, Mitsuma N, et al. Neuroprotective role of phosphodiesterase inhibitor ibudilast on neuronal cell death induced by activated microglia. Neuropharmacology 2004;46:404–11.
[14] Bhat A, Ray B, Mahalakshmi AM, Tuladhar S, Nandakumar DN, Srinivasan M, et al. Phosphodiesterase-4 enzyme as a therapeutic target in neurological disorders. Pharmacol Res 2020;160:105078.
[15] Huang Z, Liu S, Zhang L, Salem M, Greig GM, Chan CC, et al. Preferential inhibition of human phosphodiesterase 4 by ibudilast. Life Sci 2006;78:2663–8.
[16] Mancuso R, Oliván S, Mancera P, Pastén-Zamorano A, Manzano R, Casas C, et al. Effect of genetic background on onset and disease progression in the SOD1-G93A model of amyotrophic lateral sclerosis. Amyotroph Lateral Scler Off Publ World Fed Neurol Res Group Mot Neuron Dis 2012;13:302–10.
[17] Qiu H, Lee S, Shang Y, Wang W-Y, Au KF, Kamiya S, et al. ALS-associated mutation FUS-R521C causes DNA damage and RNA splicing defects. J Clin Invest 2014;124:981–99.
[18] López-Blanch R, Salvador-Palmer R, Estrela JM, Obrador E. An intercellular flow of glutathione regulated by interleukin 6 links astrocytes and the liver in the pathophysiology of amyotrophic lateral sclerosis. Antioxid Basel Switz 2021;10:2007.
[19] Weydt P, Hong SY, Kliot M, Möller T. Assessing disease onset and progression in the SOD1 mouse model of ALS. Neuroreport 2003;14:1051–4.
[20] Kong J, Xu Z. Massive mitochondrial degeneration in motor neurons triggers the onset of amyotrophic lateral sclerosis in mice expressing a mutant SOD1. J Neurosci Off J Soc Neurosci 1998;18:3241–50.
[21] Guo J, Yang X, Gao L, Zang D. Evaluating the levels of CSF and serum factors in ALS. Brain Behav 2017;7:e00637.
[22] Chen X, Hu Y, Cao Z, Liu Q, Cheng Y. Cerebrospinal fluid inflammatory cytokine aberrations in Alzheimer's disease, Parkinson's disease and amyotrophic lateral sclerosis: a systematic review and meta-analysis. Front Immunol 2018;9:2122.
[23] Lim NK-H, Moestrup V, Zhang X, Wang W-A, Møller A, Huang F-D. An improved method for collection of cerebrospinal fluid from anesthetized mice. J Vis Exp JoVE 2018:56774.
[24] Beaudet M-J, Yang Q, Cadau S, Blais M, Bellenfant S, Gros-Louis F, et al. High yield extraction of pure spinal motor neurons, astrocytes and microglia from single embryo and adult mouse spinal cord. Sci Rep 2015;5:16763.
[25] Anasagasti MJ, Martin JJ, Mendoza L, Obrador E, Estrela JM, McCuskey RS, et al. Glutathione protects metastatic melanoma cells against oxidative stress in the murine hepatic microvasculature. Hepatol Baltim Md 1998;27:1249–56.
[26] Benlloch M, Obrador E, Valles SL, Rodriguez ML, Sirerol JA, Alcácer J, et al. Pterostilbene decreases the antioxidant defenses of aggressive cancer cells in vivo: a physiological glucocorticoids- and Nrf2-dependent mechanism. Antioxid Redox Signal 2016;24:974–90.
[27] Zhang Y, Dai M, Yuan Z. Methods for the detection of reactive oxygen species. Anal Methods 2018;10:4625–38.
[28] Braman RS, Hendrix SA. Nanogram nitrite and nitrate determination in environmental and biological materials by vanadium (III) reduction with chemiluminescence detection. Anal Chem 1989;61:2715–8.
[29] Carretero J, Obrador E, Esteve JM, Ortega A, Pellicer JA, Sempere FV, et al. Tumoricidal activity of endothelial cells. Inhibition of endothelial nitric oxide production abrogates tumor cytotoxicity induced by hepatic sinusoidal endothelium in response to B16 melanoma adhesion in vitro. J Biol Chem 2001;276:25775–82.
[30] Asensi M, Sastre J, Pallardó FV, García de la Asunción J, Estrela JM, Viña J. A high-performance liquid chromatography method for measurement of oxidized glutathione in biological samples. Anal Biochem 1994;217:323–8.
[31] Obrador E, Valles SL, Benlloch M, Sirerol JA, Pellicer JA, Alcácer J, et al. Glucocorticoid receptor knockdown decreases the antioxidant protection of B16 melanoma cells: an endocrine system-related mechanism that compromises

metastatic cell resistance to vascular endothelium-induced tumor cytotoxicity. PLoS One 2014;9:e96466.
[32] Clancy RM, Miyazaki Y, Cannon PJ. Use of thionitrobenzoic acid to characterize the stability of nitric oxide in aqueous solutions and in porcine aortic endothelial cell suspensions. Anal Biochem 1990;191:138–43.
[33] Ahmed A, Dunk C, Kniss D, Wilkes M. Role of VEGF receptor-1 (Flt-1) in mediating calcium-dependent nitric oxide release and limiting DNA synthesis in human trophoblast cells. Lab Investig J Tech Methods Pathol 1997;76:779–91.
[34] Uppu RM, Pryor WA. Biphasic synthesis of high concentrations of peroxynitrite using water-insoluble alkyl nitrite and hydrogen peroxide. Methods Enzymol 1996; 269:322–9.
[35] Bergmeyer HU. Methods of Enzymatic Analysis. Verlag Chemie; 1974.
[36] Scarlett JL, Sheard PW, Hughes G, Ledgerwood EC, Ku HH, Murphy MP. Changes in mitochondrial membrane potential during staurosporine-induced apoptosis in Jurkat cells. FEBS Lett 2000;475:267–72.
[37] James AM, Wei YH, Pang CY, Murphy MP. Altered mitochondrial function in fibroblasts containing MELAS or MERRF mitochondrial DNA mutations. Biochem J 1996;318(Pt 2):401–7.
[38] Dagda RK, Rice M. Protocols for assessing mitophagy in neuronal cell lines and primary neurons. Neuromethods 2017;123:249–77.
[39] Estrela JM, Salvador R, Marchio P, Valles SL, López-Blanch R, Rivera P, et al. Glucocorticoid receptor antagonism overcomes resistance to BRAF inhibition in BRAFV600E-mutated metastatic melanoma. Am J Cancer Res 2019;9:2580–98.
[40] Ferrer P, Asensi M, Priego S, Benlloch M, Mena S, Ortega A, et al. Nitric oxide mediates natural polyphenol-induced Bcl-2 down-regulation and activation of cell death in metastatic B16 melanoma. J Biol Chem 2007;282:2880–90.
[41] Bradford MM. A rapid and sensitive method for the quantitation of microgram quantities of protein utilizing the principle of protein-dye binding. Anal Biochem 1976;72:248–54.
[42] Deng T, Hu S, Huang X-A, Song J, Xu Q, Wang Y, et al. A novel strategy for colorimetric detection of hydroxyl radicals based on a modified Griess test. Talanta 2019;195:152–7.
[43] Nishikawa M, Sato EF, Kashiba M, Kuroki T, Utsumi K, Inoue M. Role of glutathione in nitric oxide-dependent regulation of energy metabolism in rat hepatoma cells. Hepatol Baltim Md 1998;27:422–6.
[44] Hart TW. Some observations concerning the S-nitroso and S-phenylsulphonyl derivatives of L-cysteine and glutathione. Tetrahedron Lett 1985;26:2013–6.
[45] Li H, Zuo J, Tang W. Phosphodiesterase-4 inhibitors for the treatment of inflammatory diseases. Front Pharmacol 2018;9:1048.
[46] Sies H, Arteel GE. Interaction of peroxynitrite with selenoproteins and glutathione peroxidase mimics. Free Radic Biol Med 2000;28:1451–5.
[47] Harris J, Deen N, Zamani S, Hasnat MA. Mitophagy and the release of inflammatory cytokines. Mitochondrion 2018;41:2–8.
[48] Ignarro LJ, Napoli C, Loscalzo J. Nitric oxide donors and cardiovascular agents modulating the bioactivity of nitric oxide: an overview. Circ Res 2002;90:21–8.
[49] Li B, He X, Lei S-S, Zhou F-C, Zhang N-Y, Chen Y-H, et al. Hypertensive rats treated chronically with Nω-nitro-L-arginine methyl ester (L-NAME) induced disorder of hepatic fatty acid metabolism and intestinal pathophysiology. Front Pharmacol 2019;10:1677.
[50] Ragab TIM, Ali NA, El Gendy ANG, Mohamed SH, Shalby AB, Farrag A-RH, et al. Renoprotective and therapeutic effects of newly water, ethanol, and butanol ginseng fractions in hypertensive and chronic kidney disease with L-NAME. Biomed Pharmacother Biomedecine Pharmacother 2021;142:111978.
[51] Yang L, Gal J, Chen J, Zhu H. Self-assembled FUS binds active chromatin and regulates gene transcription. Proc Natl Acad Sci U S A 2014;111:17809–14.
[52] Perrotti D, Iervolino A, Cesi V, Cirinná M, Lombardini S, Grassilli E, et al. BCR-ABL prevents c-jun-mediated and proteasome-dependent FUS (TLS) proteolysis through a protein kinase CbetaII-dependent pathway. Mol Cell Biol 2000;20:6159–69.
[53] Lasiene J, Yamanaka K. Glial cells in amyotrophic lateral sclerosis. Neurol Res Int 2011;2011:718987.
[54] Pehar M, Harlan BA, Killoy KM, Vargas MR. Nicotinamide adenine dinucleotide metabolism and neurodegeneration. Antioxid Redox Signal 2018;28:1652–68.
[55] Zhao W, Xie W, Le W, Beers DR, He Y, Henkel JS, et al. Activated microglia initiate motor neuron injury by a nitric oxide and glutamate-mediated mechanism. J Neuropathol Exp Neurol 2004;63:964–77.
[56] Pehar M, Vargas MR, Robinson KM, Cassina P, Díaz-Amarilla PJ, Hagen TM, et al. Mitochondrial superoxide production and nuclear factor erythroid 2-related factor 2 activation in p75 neurotrophin receptor-induced motor neuron apoptosis. J Neurosci Off J Soc Neurosci 2007;27:7777–85.
[57] Carey AN, Fisher DR, Rimando AM, Gomes SM, Bielinski DF, Shukitt-Hale B. Stilbenes and anthocyanins reduce stress signaling in BV-2 mouse microglia. J Agric Food Chem 2013;61:5979–86.
[58] Meng X-L, Yang J-Y, Chen G-L, Wang L-H, Zhang L-J, Wang S, et al. Effects of resveratrol and its derivatives on lipopolysaccharide-induced microglial activation and their structure-activity relationships. Chem Biol Interact 2008;174:51–9.
[59] Geloso MC, Corvino V, Marchese E, Serrano A, Michetti F, D'Ambrosi N. The dual role of microglia in ALS: mechanisms and therapeutic approaches. Front Aging Neurosci 2017;9:242.
[60] Rosen DR, Siddique T, Patterson D, Figlewicz DA, Sapp P, Hentati A, et al. Mutations in Cu/Zn superoxide dismutase gene are associated with familial amyotrophic lateral sclerosis. Nature 1993;362:59–62.
[61] Neumann M, Sampathu DM, Kwong LK, Truax AC, Micsenyi MC, Chou TT, et al. Ubiquitinated TDP-43 in frontotemporal lobar degeneration and amyotrophic lateral sclerosis. Science 2006;314:130–3.
[62] Kwiatkowski TJ, Bosco DA, Leclerc AL, Tamrazian E, Vanderburg CR, Russ C, et al. Mutations in the FUS/TLS gene on chromosome 16 cause familial amyotrophic lateral sclerosis. Science 2009;323:1205–8.
[63] Lévy E, El Banna N, Baïlle D, Heneman-Masurel A, Truchet S, Rezaei H, et al. Causative links between protein aggregation and oxidative stress: a review. Int J Mol Sci 2019;20:3896.
[64] Pirie E, Oh C-K, Zhang X, Han X, Cieplak P, Scott HR, et al. S-nitrosylated TDP-43 triggers aggregation, cell-to-cell spread, and neurotoxicity in hiPSCs and in vivo models of ALS/FTD. Proc Natl Acad Sci U S A 2021;118:e2021368118.
[65] Goutman SA, Boss J, Godwin C, Mukherjee B, Feldman EL, Batterman SA. Associations of self-reported occupational exposures and settings to ALS: a case-control study. Int Arch Occup Environ Health 2022;95:1567–86.
[66] Sutedja NA, Veldink JH, Fischer K, Kromhout H, Heederik D, Huisman MHB, et al. Exposure to chemicals and metals and risk of amyotrophic lateral sclerosis: a systematic review. Amyotroph Lateral Scler Off Publ World Fed Neurol Res Group Mot Neuron Dis 2009;10:302–9.
[67] Wang L, Li C, Chen X, Li S, Shang H. Abnormal serum iron-status indicator changes in amyotrophic lateral sclerosis (ALS) patients: a meta-analysis. Front Neurol 2020; 11:380.
[68] Yamazaki T, Anraku T, Matsuzawa S. Ibudilast, a mixed PDE3/4 inhibitor, causes a selective and nitric oxide/cGMP-independent relaxation of the intracranial vertebrobasilar artery. Eur J Pharmacol 2011;650:605–11.
[69] Babu S, Hightower BG, Chan J, Zürcher NR, Kivisäkk P, Tseng C-EJ, et al. Ibudilast (MN-166) in amyotrophic lateral sclerosis- an open label, safety and pharmacodynamic trial. NeuroImage Clin 2021;30:102672.
[70] Angelopoulou E, Pyrgelis E-S, Piperi C. Emerging potential of the phosphodiesterase (PDE) inhibitor ibudilast for neurodegenerative diseases: an update on preclinical and clinical evidence. Mol Basel Switz 2022;27:8448.
[71] Takuma K, Lee E, Enomoto R, Mori K, Baba A, Matsuda T. Ibudilast attenuates astrocyte apoptosis via cyclic GMP signalling pathway in an in vitro reperfusion model. Br J Pharmacol 2001;133:841–8.
[72] Day JP, Lindsay B, Riddell T, Jiang Z, Allcock RW, Abraham A, et al. Elucidation of a structural basis for the inhibitor-driven, p62 (SQSTM1)-dependent intracellular redistribution of cAMP phosphodiesterase-4A4 (PDE4A4). J Med Chem 2011;54: 3331–47.
[73] Hennet T, Richter C, Peterhans E. Tumour necrosis factor-alpha induces superoxide anion generation in mitochondria of L929 cells. Biochem J 1993;289(Pt 2):587–92.
[74] Goossens V, Grooten J, De Vos K, Fiers W. Direct evidence for tumor necrosis factor-induced mitochondrial reactive oxygen intermediates and their involvement in cytotoxicity. Proc Natl Acad Sci U S A 1995;92:8115–9.
[75] Rolan P, Gibbons JA, He L, Chang E, Jones D, Gross MI, et al. Ibudilast in healthy volunteers: safety, tolerability and pharmacokinetics with single and multiple doses. Br J Clin Pharmacol 2008;66:792–801.
[76] Dao VT-V, Elbatreek MH, Fuchß T, Grädler U, Schmidt HHHW, Shah AM, et al. Nitric oxide synthase inhibitors into the clinic at last. Handb Exp Pharmacol 2021; 264:169–204.